IEEE Access
Multidisciplinary | Rapid Review | Open Access Journal

Received 29 July 2022, accepted 18 August 2022, date of publication 23 August 2022, date of current version 12 September 2022.

Digital Object Identifier 10.1109/ACCESS.2022.3201137

RESEARCH ARTICLE

Design Method of Constant Phase-Shifter Microwave Passive Integrated Circuit in 130-nm BiCMOS Technology With Bandpass-Type Negative Group Delay

BLAISE RAVELO[1], (Member, IEEE), MATHIEU GUERIN[2,3], (Member, IEEE), JAROSLAV FRNDA[4,5], (Senior Member, IEEE), FRANK ELLIOT SAHOA[6], GLAUCO FONTGALLAND[7], (Senior Member, IEEE), HUGERLES S. SILVA[8,9,10], (Member, IEEE), SAMUEL NGOHO[11], FAYROUZ HADDAD[2,3], (Member, IEEE), AND WENCESLAS RAHAJANDRAIBE[2,3], (Member, IEEE)

[1]School of Electronic and Information Engineering, Nanjing University of Information Science & Technology (NUIST), Nanjing, Jiangsu 210044, China
[2]CNRS, Aix-Marseille University, 13007 Marseille, France
[3]IM2NP UMR7334, University of Toulon, 13007 Marseille, France
[4]Department of Quantitative Methods and Economic Informatics, Faculty of Operation and Economics of Transport and Communication, University of Zilina, 01026 Žilina, Slovakia
[5]Department of Telecommunications, Faculty of Electrical Engineering and Computer Science, VSB—Technical University of Ostrava, 70800 Ostrava, Czech Republic
[6]Laboratoire de Physique Nucléaire et Physique de l'Environnement (LPNPE), Université d'Antananarivo, Antananarivo 101, Madagascar
[7]Applied Electromagnetic and Microwave Laboratory, Federal University of Campina Grande, Campina Grande, Paraíba 58429, Brazil
[8]Instituto de Telecomunicações, Universidade de Aveiro—Campus Universitário de Santiago, 3810-193 Aveiro, Portugal
[9]Departamento de Eletrónica, Telecomunicações e Informática, Universidade de Aveiro—Campus Universitário de Santiago, 3810-193 Aveiro, Portugal
[10]Department of Electric Engineering, University of Brasília (UnB), Brasília, Federal District 70910-900, Brazil
[11]Association Française de Science des Systèmes (AFSCET), 75013 Paris, France

Corresponding author: Mathieu Guerin (mathieu.guerin@im2np.fr)

This work was supported in part by the Ministry of Education, Youth and Sports, Czech Republic, under Grant SP2022/5; in part by the NSFC under Grant 61971230; in part by the Jiangsu Specially Appointed Professor Program and Six Major Talents Summit of Jiangsu Province under Grant 2019-DZXX-022; and in part by the Startup Foundation for Introducing Talent of the Nanjing University of Information Science & Technology.

ABSTRACT The miniaturization and application development are the expected challenges on the today engineering design research on bandpass (BP) type negative group delay (NGD) circuit. To overcome this technical limit, an innovative contribution on integrated circuit (IC) design method of BP-NGD application to design constant phase shifter (PS) in 130-nm BiCMOS technology is developed in the present paper. The BP-NGD PS microwave passive IC is topologically consisted of cascade of CLC- and RLC-resonant networks. After the S-matrix modelling, the synthesis design equations enabling to calculate each lumped component values constituting the BP-NGD PS BiCMOS are established. The design equations are expressed knowing the targeted specifications as phase shift and operating frequency. The BiCMOS design methodology including the key steps as design rule checking (DRC), layout versus schematic (LVS) and post-layout simulation (PLS) is described. The miniaturized BP-NGD PS design feasibility is verified with schematic and layout simulations with IC CMOS standard commercial software tool. A proof-of-concept (POC) of 130-nm BiCMOS BP-NGD PS operating at the center frequency $f_0 = 1.9$ GHz and bandwidth $\Delta f = 0.1$ GHz is designed and simulated. After DRC, the chip layout of miniaturized BP-NGD PS POC presents 0.407 mm^2 size. The BP-NGD PS POC exhibits constant phase shift notable value of about $\varphi_0 = -90°+/-0.4°$ under $S_{21}(f_0) = -6+/-1$ dB transmission coefficient with good flatness and reflection coefficients ($S_{21}(f_0)$ and

The associate editor coordinating the review of this manuscript and approving it for publication was Wenjie Feng.

$S_{21}(f_0)$) widely better than −10 dB. The design robustness is confirmed by 1000-trial Monte Carlo uncertainty analyses with PLS results. Because of the potential integration in wireless sensor networks (WSNs), the BP-NGD PS under study is a promising candidate for the improvement of the future 5G and 6G transceiver design.

INDEX TERMS 130-nm BiCMOS technology, integrated circuit (IC), design method, microwave circuit, passive topology, S-parameter model, bandpass (BP) negative group delay (NGD), BP-NGD application, microwave phase shifter (PS).

I. INTRODUCTION

The technological and engineering evolution trends to enhance the quality of human life and to develop the modern society. To face up the challenging societal situation, new knowledge leading to natural progress of physical science is expected. Further understanding of non-vulgar phenomena can be the most efficient solutions against the societal problems. In other words, recent research works state the existence of abnormal physical phenomena which require further study. The negative group delay (NGD) phenomenon belongs among the most counterintuitive physical phenomena which is still not well-familiar to most of electronic and communication engineers.

A. STATE OF THE ART ON THE NGD ELECTRONIC CIRCUIT DESIGN

The fascinating NGD phenomenon was initially experimented in dispersive optical media presenting negative refractive index (NRI) where the group velocity can also be negative [1], [2], [3]. The radio frequency (RF) and microwave NGD phenomenon was validated with split ring resonator (SRR) structure based NRI metamaterial circuits identified from 3-D and 2-D periodical bulk materials [4], [5]. However, the metamaterial-based microwave NGD circuits operate with significant losses. For this reason, the NGD circuit applications are literally less developed and less investigated compared to other electronic and communication functions as filter, antenna, amplifier, coupler and power combiner/divider. Last two decades, diverse topologies of NGD microwave circuits were designed and experimented [6], [7], [8], [9], [10], [11], [12]. It was demonstrated that the NGD circuits can be designed by using lumped R, L and C topologies and also microstrip topologies. In addition to the basic understanding of NGD phenomenon meaning, the main challenge at this stage was the design of low attenuation and compact NGD microwave circuit [10], [11], [12]. Moreover, despite the progressive research work from few groups around the world, the NGD engineering remains, so far, an unfamiliar concept for non-specialist RF and microwave design, manufacturing and test engineers.

An innovative fundamental theory of NGD circuit inspired from filter theory which is easy to understand for graduate students and non-specialist electronic design, fabrication, test and commercial engineers was initiated [13], [14]. The NGD circuit theory is elaborated from transfer function (TF) approach [13], [14]. It is noteworthy that the main difference is the fact that the filter is characterized from TF magnitude and the NGD is characterized from the TF group delay (GD). Based on the NGD-filter analogy, the innovative classification of low-pass (LP) [13], [14], [15], [16], [17], high-pass (HP) [13], [14], [18], [19], [20], [21], bandpass (BP) [4], [5], [6], [7], [8], [9], [10], [11], [12], [13], [14] and stop-band (SB) [13], [14], [21], [22], [23] NGD topologies are identified. These different NGD topology types are characterized from the frequency band(s) where the GD is susceptible to be negative. Behind the NGD theoretical development, there are curious questions about the application.

B. STATE OF THE ART ON THE NGD CIRCUIT-BASED PHASE SHIFTER (PS) DESIGN

Tentative RF and microwave engineering applications of NGD circuits [24], [25], [26], [27], [28], [29], [30], [31], [32], [33], [34], [35], [36] were proposed. Ones of most remarkable applications are based on the NGD equalization technique which consists of cascading positive GD (PGD) and NGD circuits [24], [25], [26], [27], [28], [29], [30], [31], [32], [33], [34], [35], [36]. The NGD equalization approach enables naturally to compensate delay and electronic component undesirable effects [25], [26], [27], [28]. By means of BP-NGD electronic function, the unfamiliar NGD equalization enables more importantly to design innovative microwave phase shifters (PSs) [29], [30], [31], [32], [33], [34]. The solution of RF and microwave PS topology can be flexibly designed with both active [29], [30], [31], [32] and passive [33], [34], [35] topologies. The main particularity of such PSs is the possibility to operate in broadband with constant value or independently with frequency [29], [30], [32], [33], [34]. This innovative PS topology can be exploited to design Hilbert filter [36] which is interesting to design higher performance transceivers (Tx-Rx). For example, the Hilbert filter is expected to be a good technological candidate to perform operation as FFT and iFFT and also to design analog and mixed modulators and demodulators for future communication front- and back-end systems. More recent study [35] highlights that by using SB-NGD function, innovative design solution of stair PSs can be performed.

Compared to the metamaterial-based microwave PS design [37] and application for front- and back-end terminals [38], [39], [40], further understanding and applicative studies of BP-NGD circuits are needed. The technical challenge slowing down the development of constant phase BP-NGD PS is the integration feasibility in miniaturized Tx-Rx

system. The prominent solution is the design in CMOS integrated circuit (IC) technology whose the feasibility for LP- [41], [42] and HP- [43] NGD circuits were recently theoretically investigated.

C. ORIGINALITY AND OUTLINE OF THE PAPER

The main novelty of the present research work is described as follows:

- The IC-based design methodology of BP-NGD PS constituted by combined capacitive-inductive-capacitive network and BP-NGD passive lumped circuits. The novel BP-NGD based PS is designed in 130-nm BiCMOS technology.
- The theoretical synthesis formulation and design approach BP-NGD based PS is designed in 130-nm BiCMOS technology. The fundamental equations allowing to calculate the lumped passive topology in function of the targeted operation frequency are established.

The present paper is organized in seven main sections as follows:

- Section II recalls the general specifications of the unfamiliar BP-NGD and positive group delay (PGD) ideal circuits.
- Section III defines the ideal analysis and also the key specifications of the behavior of the proposed BP-NGD PS from the S-matrix modelling.
- Section IV examines theoretically the analytical S-matrix models of the PGD, BP-NGD and PS lumped topologies.
- Section V reveals the synthesis equations enabling to determine the R, L and C component values from the expected specifications of the PS under study.
- Section VI is focused on the CMOS IC design methodology of the BP-NGD PS by using IC simulator Cadence® VIRTUOSO. A miniaturized BP-NGD PS proof-of-concept (POC) will be designed and studied.
- Section VII examines the verification results from calculation and simulations. Monte Carlo (MC) uncertainty analyses (UAs) are also performed to highlight the CMOS BP-NGD PS design.
- Section VIII finalizes the paper with conclusion.

II. GENERAL DESCRIPTION OF BP-NGD AND PGD FUNCTIONS

The general theoretical approach to analyze the BP-NGD PS is introduced in the present section. The introduced theory is based on S-parameter representation. The specifications of BP-NGD and also the PS are defined.

A. S-MATRIX MODELLING GENERAL DESCRIPTION

Acting as a microwave circuit, the analysis of the PS studied in this paper is essentially based on S-matrix approach. Fig. 1 represents a general configuration of two-port black box modelled by S-matrix:

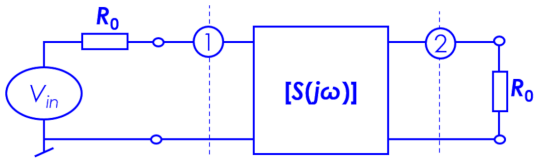

FIGURE 1. Two-port S-parameter black box.

$$[S(s)] = \begin{bmatrix} S_{11}(s) & S_{21}(s) \\ S_{21}(s) & S_{11}(s) \end{bmatrix}. \quad (1)$$

with $s = j\omega$ is the Laplace variable expressed in function of angular frequency $\omega = 2\pi f$. The S-model elaborated in the along paper is referred to the impedance $R_0 = 50\Omega$.

Acting as a symmetric circuit, we have the magnitudes of the reflection and transmission coefficients expressed as, respectively:

$$S_{11}(\omega) = |S_{11}(j\omega)| \quad (2)$$

$$S_{21}(\omega) = |S_{21}(j\omega)|. \quad (3)$$

In addition to the magnitudes, the present study will also consider:

- the phase of the transmission coefficient which is defined by:

$$\varphi(\omega) = \arg[S_{21}(j\omega)] \quad (4)$$

- the frequency dependent GD response which is defined by:

$$GD(\omega) = -\frac{\partial\varphi(\omega)}{\partial\omega}. \quad (5)$$

When the last quantity is negative, the S-parameter presents an unfamiliar NGD behavior. The next subsection recalls the main specifications of BP-NGD type circuits.

B. SPECIFICATIONS OF TYPICAL BP-NGD FUNCTION

A circuit can be classified as typical BP-NGD function if we can find an angular frequency, ω, from the transmission coefficient GD respecting the condition:

$$GD(\omega) < 0. \quad (6)$$

An ideal response of BP-NGD function can be represented by:

- The cut-off angular frequencies, ω_1 and ω_2, as depicted by Fig. 2(a), as roots of equation:

$$GD(\omega) = 0. \quad (7)$$

- By taking a real negative parameter t_n, the ideal GD response can be negative as defined by:

$$GD(\omega_1 \leq \omega \leq \omega_2) = t_n < 0. \quad (8)$$

- By taking the maximal reflection coefficient $0 < A_{max} < 1$, we have the ideal response displayed as plotted in Fig. 2(b):

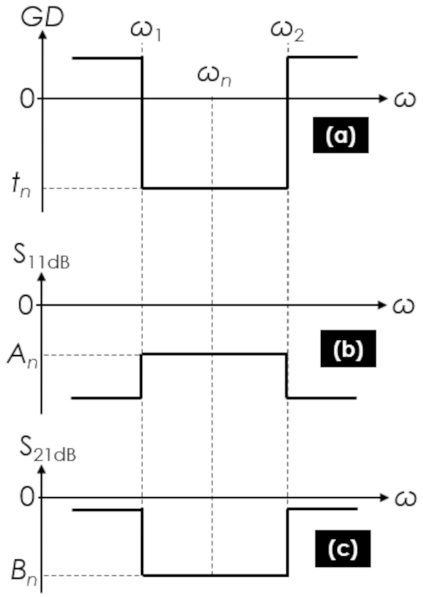

FIGURE 2. (a) GD, (b) refection and (c) transmission coefficient responses of typical BP-NGD function.

$$S_{11}(\omega_1 \leq \omega \leq \omega_2) = A_n \leq A_{\max}. \tag{9}$$

- And by taking the minimal transmission coefficient $0 < B_{min} < 1$, we have the ideal response as shown in Fig. 2(c):

$$S_{21}(\omega_1 \leq \omega \leq \omega_2) = B_n \geq B_{\min}. \tag{10}$$

For the case of BP-NGD circuit, the bandwidth is defined by:

$$\Delta\omega = \omega_2 - \omega_1. \tag{11}$$

To design an ideal PS, the ideal S-matrix model of BP-NGD in frequency band $[\omega_1, \omega_2]$ with:

$$\left|S_{11,NGD}(j\omega)\right| = \left|S_{22,NGD}(j\omega)\right| \approx 0. \tag{12}$$

Therefore, the BP-NGD S-matrix can be formulated by:

$$[S_{NGD}(j\omega)] = \begin{bmatrix} 0 & S_{21,NGD}(j\omega) \\ S_{21,NGD}(j\omega) & 0 \end{bmatrix}. \tag{13}$$

The S-matrix presents the associated transmission coefficient expressed as:

$$S_{21,NGD}(j\omega) = B_n \cdot \exp\left[j(\varphi_n - \omega \cdot t_n)\right] \tag{14}$$

with $0 < B_n < 1$ and initial phase shift:

$$\varphi_n = \varphi_{NGD}(\omega_1). \tag{15}$$

In opposite to the present case, the PGD circuit specifications will be elaborated in the next section.

C. SPECIFICATIONS OF THE PGD FUNCTION BEHAVIOR

The PGD function operates as typical true time delay (TTD) circuit assumed to work in the frequency band defined by limits ω_1 and ω_2 with $\omega_1 < \omega_2$ which is the same as the frequency band of the previously described BP-NGD function. By taking real positive t_p, the ideal GD diagram can be represented by Fig. 3 specified by:

$$GD(\omega_1 \leq \omega \leq \omega_2) = t_p > 0. \tag{16}$$

The PGD is expected to present the same specifications in terms of reflection and transmission coefficients as the BP-NGD ones plotted in Fig. 2(b) and Fig. 2(c), with $A_p = A_n$ and $B_p = B_n^2$, respectively. The GD diagram shown by Fig. 3 enables to express the phase shift associated to the PGD that within frequency band $[\omega_1, \omega_2]$. Accordingly, the ideal S-matrix model of PGD under ideal condition:

$$\left|S_{11,PGD}(j\omega)\right| = \left|S_{22,PGD}(j\omega)\right| \approx 0. \tag{17}$$

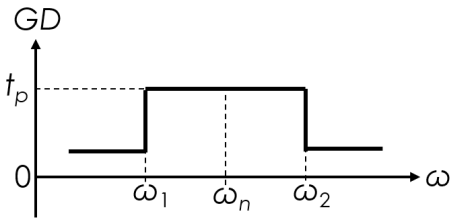

FIGURE 3. GD diagram of PGD function constituting the PS.

The associated S-matrix should be:

$$[S_{PGD}(j\omega)] = \begin{bmatrix} 0 & S_{21,PGD}(j\omega) \\ S_{21,PGD}(j\omega) & 0 \end{bmatrix} \tag{18}$$

which presents the associated transmission coefficient expressed as:

$$S_{21,PGD}(j\omega) = B_p \cdot \exp\left[j(\varphi_p - \omega \cdot t_p)\right] \tag{19}$$

with $0 < B_p < 1$ and initial phase shift:

$$\varphi_p = \varphi_{PGD}(\omega_1). \tag{20}$$

The next section describes the proposed PS theorization from the previously defined BP-NGD and PGD characterization.

III. GENERAL DESCRIPTION OF THE BP-NGD BASED CONSTANT PS

The fundamental theory of the constant or independent of frequency PS is described in the present subsection. The ideal representation of the constituting PGD and NGD circuit is introduced. The ideal main specifications and the analytical approach from the S-parameter operation are defined.

A. S-PARAMETER IDEAL ANALYSIS OF THE BP-NGD FUNCTION BASED PS

The BP-NGD PS under study is composed cascaded PGD and NGD circuits. The analysis is elaborated based on the

frequency domain representation. The two identical NGD circuits are intercalated by PGD one. The topological solution to design this PS, we proposed the two-port topology introduced by Fig. 4. Since the reflection coefficients are negligible under conditions (12) and (17), the S-matrix modelling of this synoptic diagram is the product:

$$[S(j\omega)] = [S_{NGD}(j\omega)] \times [S_{PGD}(j\omega)] \times [S_{NGD}(j\omega)]\,. \quad (21)$$

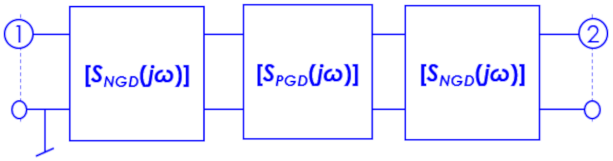

FIGURE 4. Two-port black box of frequency-independent PS constituted by PGD and NGD circuits in cascade.

Substituting the S-matrix of equation (13) and equation (18) into the previous relation, it yields the PS following ideal model:

$$[S(j\omega)] = \begin{bmatrix} 0 & S_{21}(j\omega) \\ S_{21}(j\omega) & 0 \end{bmatrix} \quad (22)$$

where the overall transmission coefficient ideally expressed as follows:

$$S_{21}(j\omega) = S_{21,NGD}(j\omega) \cdot S_{21,PGD}(j\omega) \cdot S_{21,NGD}(j\omega). \quad (23)$$

It yields the phase shift analytical expression of the next subsection.

B. PHASE SHIFT ANALYTICAL EXPRESSION

Substituting the transmission coefficients given by equation (14) and equation (19) into the previous one, we have:

$$S_{21}(j\omega) = B_n^2 B_p \exp\left\{j\left[2\varphi_n + \varphi_p - \omega(2t_n + t_p)\right]\right\}. \quad (24)$$

It means that the associated phase shift $\varphi_{PS}(\omega) = \arg[S_{21}(j\omega)]$ is given by:

$$\varphi_{PS}(\omega) = 2\varphi_n + \varphi_p - \omega(2t_n + t_p). \quad (25)$$

To generate a frequency independent PS within frequency band $[\omega_1, \omega_2]$, the phase shift must be expressed as:

$$\varphi_{PS}(\omega) = \varphi_0 = \text{Constant}. \quad (26)$$

By identification coefficients of equations (25) and (26), we have:

- The PS GD $GD_{PS}(\omega) = -\partial\varphi_{PS}(\omega)/\partial\omega$ as defined in equation (5) becomes:

$$GD_{PS}(\omega) = t_p + 2t_n = 0. \quad (27)$$

  which implies:

$$t_p = -2t_n. \quad (28)$$

- The independent frequency phase value:

$$\varphi_0 = 2\varphi_n + \varphi_p. \quad (29)$$

More illustrative comprehension about the constant phase shift aspect can be reached with graphical representation of phase diagram.

C. PHASE DIAGRAM ANALYSIS OF THE BP-NGD BASED PS

The previous analytical approach enables to plot the ideal behavior of the BP-NGD PS understudy. We also recall that the PS is expected to operate within frequency band $[\omega_1, \omega_2]$. We can denote $\omega_0 \in [\omega_1, \omega_2]$ a particular operating angular frequency. According to such particular characteristics, we can realize a frequency independent PS illustrated from algebraic operation based on PGD and NGD phase plot shown by Fig. 5(a). Following the ideal case behavior, it is noteworthy that the BP-NGD PS should present:

- A phase shift equal to constant $\varphi_{PS}(\omega) = \varphi_0$ which is equal to constant or does not depend to the frequency as stated by equation (26) and depicted by Fig. 5(a).
- A zero delay in the working frequency band of the study as stated by equation (27) and highlighted by Fig. 5(b).

Before the investigation of POC, a concrete design of the proposed PS with RLC-network based lumped circuit is investigated in the next subsection.

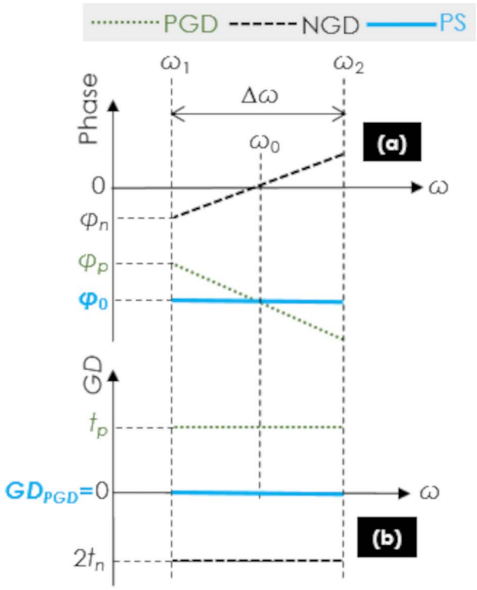

FIGURE 5. (a) Phase and (b) GD responses of PGD, NGD, and frequency-independent PS ideal function.

IV. S-PARAMETER MODEL OF PGD AND NGD PASSIVE CIRCUITS UNDER CONSIDERATION

The S-parameter models of the elementary circuits constituting the PGD, NGD and constant PS circuits are developed in this section.

A. S-PARAMETER MODELLING OF PGD TOPOLOGY

Fig. 6 represents the schematic of the PGD passive two-port circuit. It acts as a π-topology composed of two identical C_p-parallel capacitors connected at the input/output accesses and L_p-series inductor. This passive cell can be named CLC-circuit also in the rest of the paper.

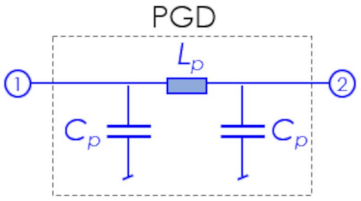

FIGURE 6. Schematic of two-port PGD circuit constituting the BP-NGD PS under study.

The PGD-topology equivalent impedance matrix is given by:

$$[Z_{PGD}(s)] = \frac{\begin{bmatrix} 1+L_pC_ps^2 & 1 \\ 1 & 1+L_pC_ps^2 \end{bmatrix}}{2+C_ps(2+L_pC_ps^2)}. \quad (30)$$

The S-matrix model is calculated from Z-to-S transform relationship:

$$[S_{PGD}(s)] = \begin{Bmatrix} \{[Z_{PGD}(s)] - R_0\,[I_{2-D}]\} \times \\ \{[Z_{PGD}(s)] + R_0\,[I_{2-D}]\}^{-1} \end{Bmatrix} \quad (31)$$

with 2-D identity matrix:

$$[I_{2-D}] = \begin{bmatrix} 1 & 0 \\ 0 & 1 \end{bmatrix} \quad (32)$$

Accordingly, we have the reflection and transmission coefficient expressions of the following PGD S-matrix:

$$S_{11,PGD}(s) = \frac{s\left[L_p - R_0^2C_p(2+L_pC_ps^2)\right]}{D_{PGD}(s)} \quad (33)$$

$$S_{21,PGD}(s) = \frac{2R_0}{D_{PGD}(s)} \quad (34)$$

where:

$$D_{PGD}(s) = (1+R_0C_ps)\left[R_0(2+L_pC_ps^2)+L_ps\right]. \quad (35)$$

These analytical relations will be exploited to elaborate the analysis and design method in the following subsection.

B. BP-NGD S-PARAMETER MODELLING AND NALYSIS

The BP-NGD topology is comprised of simple RLC-series network as parallel impedance. The two-port cell is presented by Fig. 7.

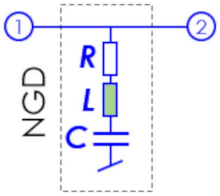

FIGURE 7. BP-NGD passive cell employed in this paper to design the constant PS.

The equivalent matrix impedance associated to the NGD passive topology is written as:

$$[Z_{NGD}(s)] = Z(s) \times \begin{bmatrix} 1 & 1 \\ 1 & 1 \end{bmatrix} \quad (36)$$

with:

$$Z(s) = R + L\,s + \frac{1}{C\,s}. \quad (37)$$

The associated S-matrix model is established from Z-to-S matrix transform from relationship as expressed in equation (31). Accordingly, we have the reflection and transmission coefficient expressions of the following S-matrix of the NGD passive cell:

$$S_{11,NGD}(s) = \frac{-R_0}{R_0+2Z(s)} \quad (38)$$

$$S_{21,NGD}(s) = \frac{2Z(s)}{R_0+2Z(s)}. \quad (39)$$

The model of the PGD and NGD combined cells is elaborated in the next subsection.

C. π-TOPOLOGY S-PARAMETER MODELLING OF PS CIRCUIT

Figs. 8 represent the concrete circuit for designing PS passive topology. It is constituted by the combined PGD and NGD circuits schematized by the general π-topology shown by Fig. 8(a). The detailed configuration of the BP-NGD PS circuit including all the lumped components is depicted by Fig. 8(b).

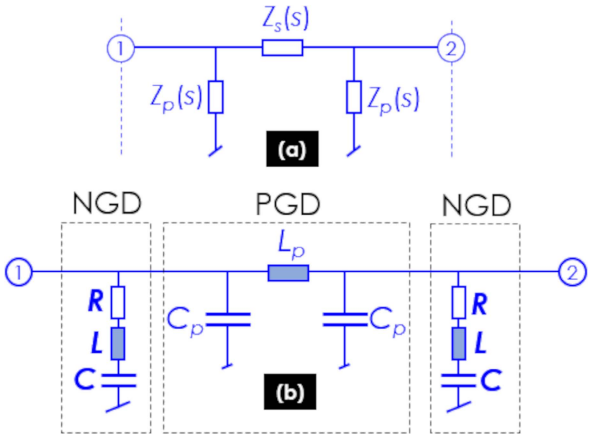

FIGURE 8. (a) Equivalent impedance based π-topology and (b) two-port black box of frequency-independent PS constituted by PGD and NGD circuits in cascade.

The passive topology of the PS is composed of two identical Z_p-parallel impedances connected at the input/output accesses and Z_s-series impedance analytically given by:

$$\begin{cases} Z_s(s) = L_s\,s \\ Z_p(s) = \dfrac{Z(s)}{1+C\,s\,Z(s)}. \end{cases} \quad (40)$$

The BP-NGD PS-topology equivalent impedance matrix is given by:

$$[Z_{PS}(s)] = \Xi(s)\begin{bmatrix} Z_s(s)+Z_p(s) & Z_p(s) \\ Z_p(s) & Z_s(s)+Z_p(s) \end{bmatrix} \quad (41)$$

with:

$$\Xi(s) = \frac{Z_p(s)}{Z_s(s) + 2Z_p(s)}. \quad (42)$$

By means of Z-to-S matrix transform, we have the reflection and transmission coefficient expressions of the following S-matrix of the BP-NGD PS passive cell:

$$S_{11,PS}(s) = \frac{Z_s(s)Z_p^2(s) - R_0^2\left[Z_s(s) + Z_p(s)\right]}{D_{PS}(s)} \quad (43)$$

$$S_{21,PS}(s) = \frac{2R_0Z_p^2(s)}{D_{PS}(s)} \quad (44)$$

with:

$$D_{PS}(s) = \left\{ \begin{array}{l} \left[R_0 + 2Z_p(s)\right] \\ \left\{R_0\left[Z_s(s) + Z_p(s)\right] + Z_s(s)Z_p(s)\right\} \end{array} \right\}. \quad (45)$$

Before the design methodology of BP-NGD PS in CMOS technology, the synthesis formulas of lumped components will be investigated in the following section.

V. SYNTHESIS FORMULAS OF THE BP-NGD CONSTANT PS

This section describes the main design formulas established from the previous analyses. The values of resistor, inductor and capacitor components constituting the BP-NGD PS are addressed in function of the targeted specifications.

A. HYPOTHESES FOR THE PRESENT BP-NGD PS ANALYSES

For the sake of the mathematical complexity, let us take a real positive parameter $A \ll 1$ as the hypothetical reflection loss. The synthesis of the proposed PS in the present paper is performed under matching conditions of PGD and NGD reflection coefficients:

$$\left\{ \begin{array}{l} \left|S_{11,PGD}(j\omega)\right| = \left|S_{22,PGD}(j\omega)\right| = A \\ \left|S_{11,NGD}(j\omega)\right| = \left|S_{22,NGD}(j\omega)\right| = A. \end{array} \right. \quad (46)$$

Consequently, we expect to have the PS access matching with respect to equation:

$$\left|S_{11,PS}(j\omega)\right| = \left|S_{22,PS}(j\omega)\right| = A. \quad (47)$$

Based on such hypothesis, the BP-NGD PS transmission coefficient can be simply approximated by the following product:

$$S_{21,PS}(j\omega) \approx S_{21,NGD}(j\omega) \cdot S_{21,PGD}(j\omega) \cdot S_{21,NGD}(j\omega). \quad (48)$$

Based on such assumption, the syntheses of our PS consist in determining lumped component with respect to the targeted specifications. The design approach can be explored from analyses from PGD and NGD circuits. The analytical elaboration of the last two ones are examined in the two next subsections.

B. DESIGN EQUATIONS OF THE PGD CIRCUIT CONSTITUTING COMPONENTS

The analysis and synthesis of the PGD circuit is elaborated in the present subsection.

1) PGD CIRCUIT ANALYSIS AT THE WORKING FREQUENCY

First of all, the PGD circuit can be analyzed by the examination of magnitude of reflection coefficient expressed in equation (33) and the phase of transmission coefficient expressed in equation (34). We can choose as particular angular frequency:

$$\omega = \frac{1}{\sqrt{L_pC_p}}. \quad (49)$$

Secondly, it is important to underline that at this angular frequency, the PGD circuit shown by Fig. 6 is in phase quadrature:

$$\varphi_{PGD}(\omega_0) = -\pi/2. \quad (50)$$

The PGD circuit synthesis consists practically in determining the constituting components inductor L_p and capacitor C_p to target the particular operation angular frequency and reflection coefficient $A \ll 1$ by solving equations:

$$\omega = \omega_0 \quad (51)$$

$$\left|S_{11,PGD}(j\omega_0)\right| = A. \quad (52)$$

In this case, we have:

- The transmission coefficient written in equation (34) becomes:

$$\left|S_{21,PGD}(j\omega_0)\right| = \sqrt{1 - A^2}. \quad (53)$$

- The GD defined in equation (5) applied to equation (34) becomes:

$$GD_{PGD}(\omega_0) = t_p \quad (54)$$

which is given by:

$$t_p = \frac{2\sqrt{1 - A^2}}{\omega_0}. \quad (55)$$

These analytical equations serve to characterize our PGD circuit as described in the following paragraph.

2) GRAPHICAL ANALYSIS

By using equation (55), the variation of the PGD GD and working frequency product versus reflection coefficient A is plotted in Fig. 9(a). We can see that the product variation is not significant when A increases to -40 dB to -10 dB. Consequently, based on such increase of reflection coefficient, we see that the GD-working frequency product decreases from 0.318 to 0.302.

The cartographies of the PGD GD t_p versus pair working frequency varying from $f_{min} = 0.5$ GHz and $f_{max} = 2.5$ GHz and reflection coefficient A is displayed in Fig. 9(b). In the considered range of pair (A, f_0), we emphasized that t_p is decreasing from 0.637 ps to 120 ps inversely to f_0 and A.

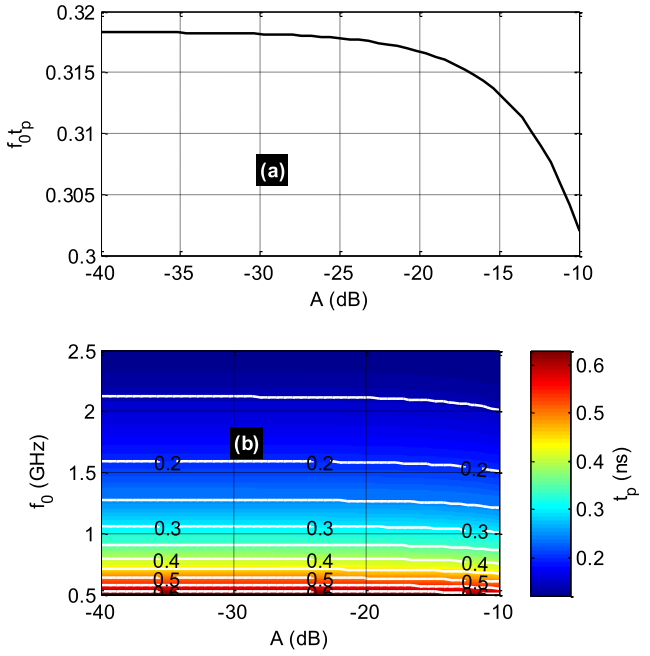

FIGURE 9. Plots of PGD (a) GD-working frequency and (c) GD cartography versus pair (A, f_0).

3) SYNTHESIS FORMULAS

The design equations of the PGD circuit are established by inversing the equation of reflection coefficient and GD. Accordingly, the PGD-circuit synthesis formulas derived from the previous equations are:

$$L_p = \frac{R_0}{\omega_0}\sqrt{\frac{1+A}{1-A}} \tag{56}$$

$$C_p = \frac{\sqrt{\frac{1-A}{1+A}}}{R_0\omega_0}. \tag{57}$$

The other formulas for calculating the other components of the PS are established from the analysis of the BP-NGD circuit and the PS shown by Fig. 7 and Fig. 8, respectively. The BP-NGD circuit analysis are introduced in the following subsection.

C. ANALYSIS AND SYNTHESIS OF BP-NGD CIRCUIT CONSTITUTING COMPONENTS

As stated in [29], [30], [31], [32], [33], [34], [35], and [36], the BP-NGD circuit must operate in opposite phase of the PGD one. The NGD block ideal specification will be defined in the following paragraph.

The BP-NGD circuit shown in Fig. 7 was analyzed by the examination of magnitude of reflection coefficient expressed in equation (38) and the GD associated to the transmission coefficient expressed in equation (39) at the particular angular frequency:

$$\omega = \frac{1}{\sqrt{LC}}. \tag{58}$$

It should be pointed out that at this angular frequency, the NGD circuit presents the phase from equation (39) equal to:

$$\varphi_{NGD}(\omega_0) = 0. \tag{59}$$

In this case, we have:

- The reflection coefficient written in equation (38) becomes:

$$\left|S_{11,NGD}(j\omega_0)\right| = \frac{R_0}{R_0+2R}. \tag{60}$$

- The transmission coefficient written in equation (39) becomes:

$$\left|S_{11,NGD}(j\omega_0)\right| = \frac{R_0}{R_0+2R}. \tag{61}$$

- The GD defined in equation (5) applied to equation (39) becomes:

$$GD_{NGD}(\omega_0) = t_n. \tag{62}$$

which is given by:

$$t_n = \frac{-2R_0L}{R(R_0+2R)}. \tag{63}$$

The BP-NGD circuit synthesis equations are established in the following subsection.

D. ELABORATION OF NGD CIRCUIT COMPONENT SYNTHESIS

The NGD circuit synthesis is naturally the calculations of the constituting components resistor R, inductor L and capacitor C to target:

- The particular operation angular frequency as stated in equation (51).
- The reflection coefficient verifying:

$$\left|S_{11,NGD}(j\omega_0)\right| = A \tag{64}$$

- The GD equalized from equation (28) which leads to the equation:

$$\frac{2R_0L}{R(R_0+2R)} = \frac{t_p}{4} \tag{65}$$

Lastly, the NGD-circuit synthesis formulas derived from the previous equations are:

$$R = \frac{R_0(1-A)}{2A} \tag{66}$$

$$L = \frac{R_0}{8A^2\omega_0}\sqrt{\frac{1+A}{1-A}} \tag{67}$$

$$C = \frac{8A^2}{R_0\omega_0}\sqrt{\frac{1-A}{1+A}}. \tag{68}$$

Knowing the resistor synthesis equation, the transmission coefficient written in equation (34) becomes:

$$\left|S_{21,NGD}(j\omega_0)\right| = 1-A. \tag{69}$$

Further insight on the BP-NGD characteristics can be established from these R, L and C component synthesis equations.

E. BP-NGD CIRCUIT BANDWITH VERSUS REFLECTION COEFFICIENT

The analysis of the BP-NGD bandwidth is described in the present subsection.

1) ANALYTICAL EXPRESSION

The GD of the BP-NGD circuit shown in Fig. 7 can be expressed from the transmission coefficient introduced in equation (39) and definition (5). The NGD cut-off angular frequencies are determined by solving equation (7). Following these analytical actions, it can be derived from synthesis equations (66), (67) and (68), the NGD cut-off frequencies versus reflection coefficient and center frequency given by:

$$\omega_1 = \omega_0\sqrt{\frac{1+8A^3(A-2)+A\left[1+4(a-1)\sqrt{\lambda}\right]}{A+1}} \quad (70)$$

$$\omega_2 = \sqrt{\frac{1+8A^3(A-2)+A\left[1+4(1-a)\sqrt{\lambda}\right]}{A+1}} \quad (71)$$

with:

$$\lambda = 1+A+4A^2(A-1)^2. \quad (72)$$

It implies the NGD relative BW which is defined $\Delta\omega/\omega_0 = \Delta f/f_0$ by formula:

$$\frac{\Delta f}{f_0} = \frac{4A(1-A)\left[2A(A-1)+\sqrt{\lambda}\right]}{\sqrt{(1+A)\left\{1+A\left[1+4(A-1)\left[2A^2(A-1)+\sqrt{\lambda}\right]\right]\right\}}}. \quad (73)$$

2) GRAPHICAL ANALYSIS

For further insight about the variation of previously expressed parameters, graphical analyses of the NGD relative bandwidth and transmission coefficient are performed in the present paragraph when A increases from -40 dB to -10 dB. Accordingly, Fig. 10(a) represents the monotonic variation of the NGD BW expressed by equation (70). We find that this relative frequency increases almost linearly from about 4% to 75.4%. However, the transmission coefficient variation decreases from -3.3 dB to -0.09 dB as witnessed by in Fig. 10(b).

Before the numerical verification of the established microwave theory feasibility, the next subsection describes the design of POC to be investigated and also the associated methodology for 130-nm BiCMOS BP-NGD PS.

VI. METHODOLOGY AND DESCRIPTION OF 130-nm BiCMOS BP-NGD PS DESIGN

The present section describes the CMOS design methodology of the BP-NGD PS topology. A POC designed in 130-nm BiCMOS technology by using an IC design and simulation commercial tool will be introduced.

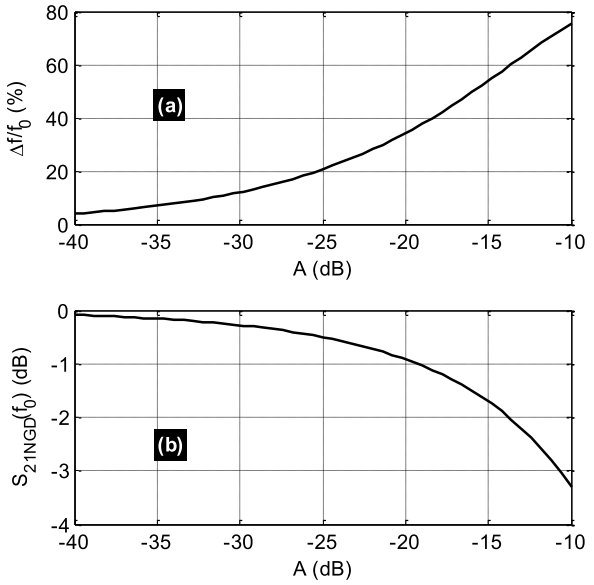

FIGURE 10. Variations of (a) NGD BW and (b) transmission coefficient versus reflection coefficient at the operation frequency.

A. DESIGN METHODOLOGY OF THE BP-NGD PS IN CMOS TECHNOLOGY

Similar to the CMOS design method of NGD ICs introduced in [41], [42], and [43], the proposed BP-NGD PS one should start from the targeted specifications to the final layout design. The main actions behind the design methodology of BP-NGD PS ICs are indicated by the design flow depicted by Fig. 11. The proposed six principal steps of the CMOS IC design can be described as follows:

- **Step 1:** The choice of the BP-NGD PS specifications as phase shift (fixed to $\varphi_0 = -90°$ for the present study) working frequency and reflection loss which is linked to the attenuation. The designer can refer to the specifications plotted by Figs. 5.
- **Step 2:** The ideal values of resistor, inductor and capacitor constituting the BP-NGD PS IC should be calculated. For this step, the design engineers can use formulas (56), (57), (66), (67) and (68).
- **Step 3:** The previously calculated values must be verified in the component library of the simulation software (for the present study, Cadence-VURTUOSO®). Then, the feasibility of the BP-NGD PS CMOS IC design should be investigated by the comparison between the calculated results of S-parameter simulations.
- **Step 4:** The layout design should begin in the present step after schematic ideal simulation. The BP-NGD PS CMOS IC must respect the design rule check (DRC) with high Ohmic unsalicided N+poly resistor and symmetrical high current spiral inductor. The DRC ensures that the design can be manufactured within the limits of production process. The layout versus schematic (LVS) of BP-NGD PS CMOS IC must be performed. The LVS

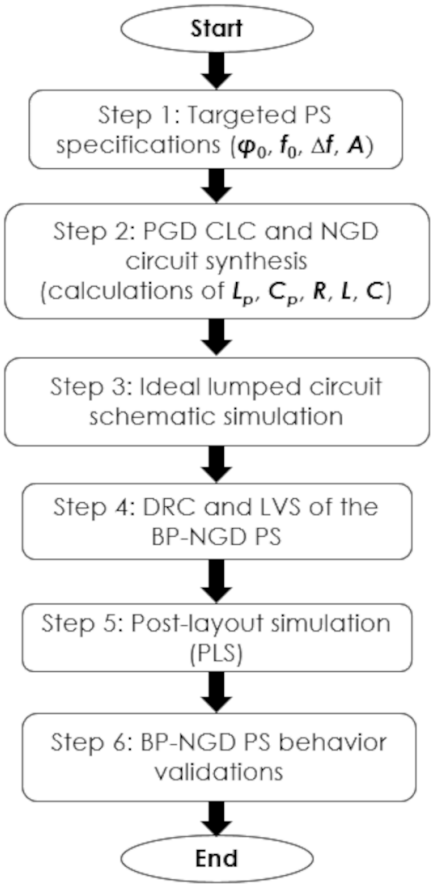

FIGURE 11. Design flow of BP-NGD PS CMOS IC.

consists in evaluating the differences by comparing the results of circuit diagram with its layout.

- **Step 5:** The effects of parasitic capacitances and resistors on the BP-NGD PS CMOS IC performances can be investigated in this present step. In all, the simulations should focus on the circuit layout. Further modifications on the IC design maybe proposed in order to meet the expected constant PS performances.
- **Step 6:** The final action of the BP-NGD PS CMOS IC design is the post-layout simulation (PLS). Any modifications can be made, in particular at the layout level, to improve the results All the rules of DRC should be validated and the result acceptability can be assessed following the targeted specifications defined in Step 1.

Following the elaborated design methodology, the BP-NGD PS POC is designed in 130-nm BiCMOS technology in the following section.

B. DESCRIPTION OF THE BP-NGD PS POC DESIGN

The POC design of the BP-NGD PS under study in 130-nm BiCMOS technology is investigated in the present subsection. The different steps of workflow indicated by Fig. 11 were followed during the design.

The BP-NGD PS specifications are arbitrarily chosen in order to highlight the microwave CMOS IC design feasibility study. The main specifications including the consideration of the investigation frequency band are indicated in Table 1. The IC design focuses first on the BP-NGD and PGD circuits. Then, the combined circuit is designed to analyze the PS behavior. As result, Fig. 12 represents the schematics of the PGD, NGD and PS POC designed in the environment of the ADS® electronic and RF/microwave simulation tools from Keysight technologies®.

TABLE 1. Specifications of the BP-NGD PS Circuit POC.

Circuit	Parameter	Arbitrary chosen value
PS	Center frequency	f_0=1.9 GHz
	Phase shift	φ_0=90°
	Bandwidth	Δf=0.2 GHz
	Reflection coefficient	-25 dB
PGD	Center frequency	f_p=f_0
	PGD value	t_p=-156 ps
	Reflection coefficient	A_p=-15 dB
	Transmission coefficient	B_p=-1 dB
NGD	Center frequency	f_n=f_0
	NGD value	t_n=-78 ps
	Reflection coefficient	A_n=-15 dB
	Transmission coefficient	B_n=-6 dB

The component values of resistor, inductor and capacitor constituting the constant phase BP-NGD PS were calculated from formulas (56), (57), (66), (67) and (68). The calculated results of POC PGD and NGD R, L and C parameters are addressed in Table 2.

TABLE 2. Parameters of the PGD and NGD circuits constituting the PS.

Circuit	Parameter	Calculated components
PGD	Inductor	L_p=5 nH
	Capacitor	C_p=1.4 pF
NGD	Resistor	R=116 Ω
	Inductor	L=20 nH
	Capacitor	C=0.35 pF

The BiCMOS BP-NGD PS design is described in the following subsection.

C. DESCRIPTION OF THE BP-NGD PS LAYOUT OF CMOS IC DESIGN

The CADENCE VIRTUOSO® design of the PS schematic is displayed in Fig. 13. The STMicroelectronics 130-nm BiCMOS manufacturing process was chosen as main reference for the present microwave PS design because of its component integration potential in the range of desired specification values.

Due to the relatively large size of the components, expensive manufacturing processes such as 28 nm-FDSOI are not needed. Fig. 14 displays the layout of the designed CMOS IC PS chipset. This PS POC layout is designed with 1.1 mm × 0.37 mm size. The resistors and inductor were

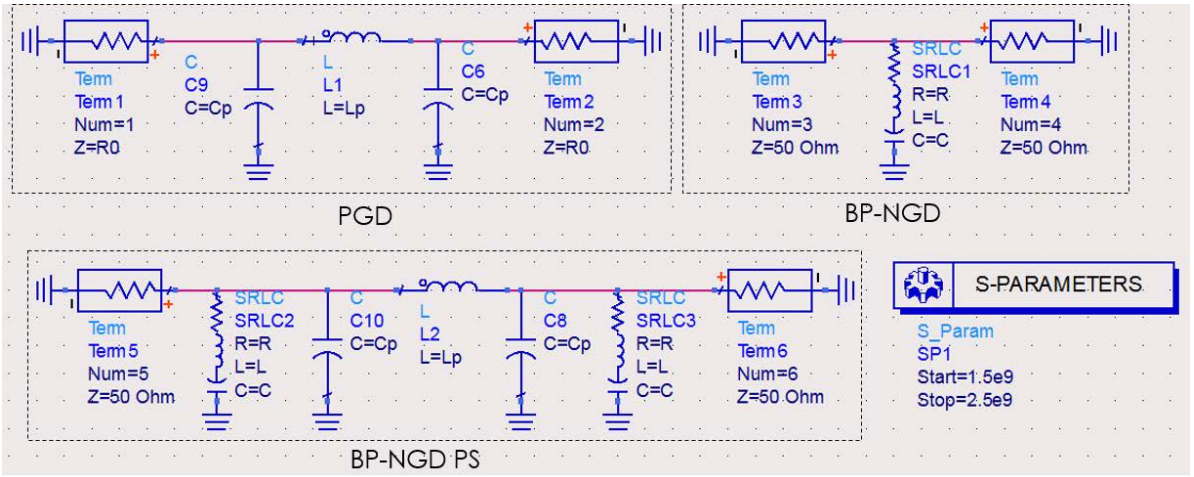

FIGURE 12. ADS® schematic of the BP-NGD PS POC.

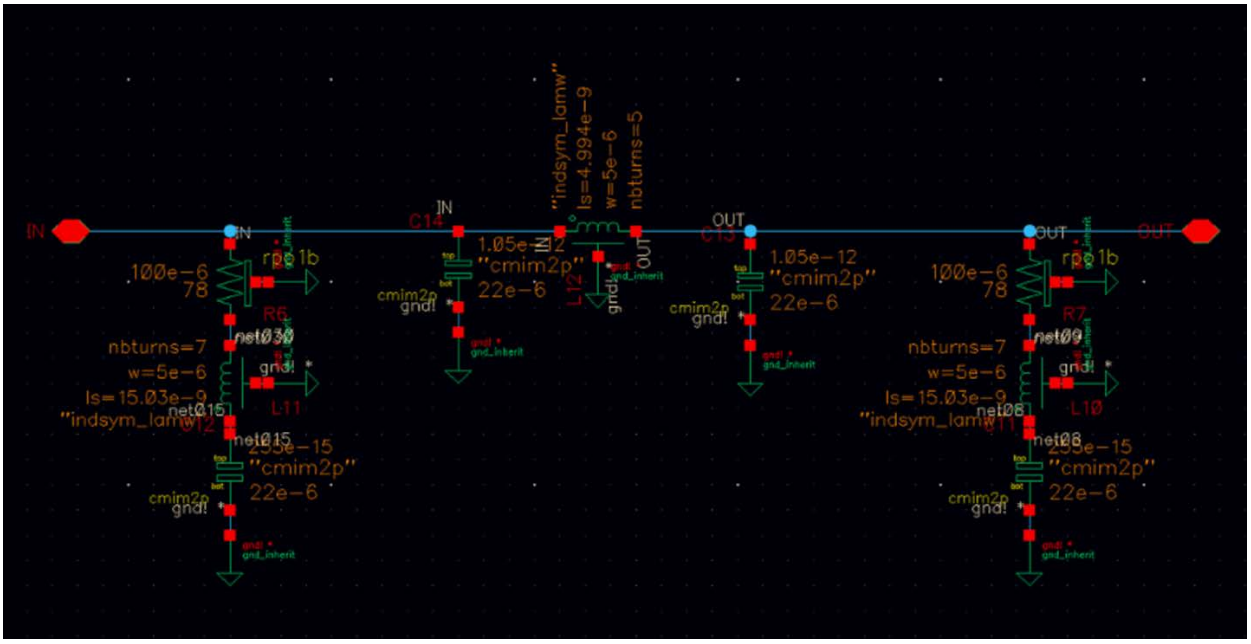

FIGURE 13. Cadence® schematic of the BP-NGD PS POC.

expected to be implemented under the manufacturing process minimum square area. The SISO circuit whole layout area is occupied by the two resistors in left and the large spiral inductor. The 100 μm $\times$ 4.9 μm size resistors are implemented in 100-nm thickness poly-Si on 4.5-relative permittivity dielectric insulator. Each resistor is guard-ring surrounded in order to ensure their polarization and the ground plane connection through the dielectric substrate.

The inductor is implemented in Al-metal spiral octagon with 0.0145 mm^2 surface over 1 μm thickness. All the layout component interconnections are Cu-based interconnect metallization with 0.1 μm thickness.

The range of the geometrical parameters (width, length, number of turns, diameter, Silicium area) of the considered resistor and inductor layouts in function of the constituting materials are addressed in Table 3 and Table 4, respectively. The minimal resonance frequency is also indicated.

VII. VERIFICATION RESULTS AND MC UNCERTAINTY ANALYSES OF THE DESIGNED 130-nm BiCMOS POC

The present section deals with the numerical verification and state of the art study of the BP-NGD PS topology. The frequency dependent BP-NGD PS behavior will be discussed. The compared and obtained results are from:

- Calculations computed ideal circuit models from MATLAB®,

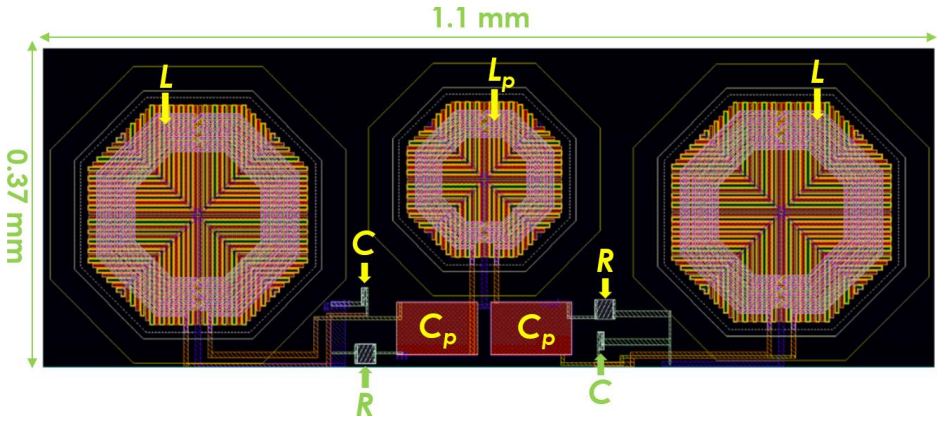

FIGURE 14. Chip Cadence-VIRTUOSO® layout (1.1 mm x 0.37 mm=0.407 mm^2) of BP-NGD PS POC.

TABLE 3. Ranges of geometrical parameters of the used designed 130-nm BiCMOS resistors.

Description	Type of resistor design	Width, w		Length, d		Resistor value	
Parameter	Unsalicided N+active resistor	w_{min}	w_{max}	d_{min}	d_{max}	R_{min}	R_{max}
Value	rpo1b	1 µm	100 µm	3 µm	100 µm	4 Ω	13 kΩ

TABLE 4. Ranges of geometrical parameters of the used designed inductor.

Description	Type of inductor	Width, w		Diameter, ϕ		Number of turns, N		Inductor value	
Parameter	Inductor symmetrical high current	w_{min}	w_{max}	ϕ_{min}	ϕ_{max}	N_{min}	N_{max}	L_{min}	L_{max}
Value	indsym_lamw	5 µm	12 µm	53 µm	163 µm	2	9	3.8 nH	25.8 nH

Description	Type of inductor	Si area, S		Resonance frequency	
Parameter	Inductor symmetrical high current	S_{min}	S_{max}	f_{min}	f_{max}
Value	indsym_lamw	0.0144 mm²	0.0961 mm²	3.33 GHz	91.4 GHz

- Simulation of ideal schematic circuits with the ADS® electronic and RF/microwave simulation tool from Keysight technologies®,
- and IC design and simulation of CMOS IC BP-NGD PS having schematic shown in Fig. 13 and layout shown in Fig. 14 with CADENCE VIRUTOSO®.

The presented results are generated in the frequency band delimited by $f_{min} = 1.5$ GHz and $f_{max} = 2.3$ GHz which contains intentionally the expected working frequency $f_0 = 1.9$ GHz. The CADENCE VIRTUOSO® MC uncertainty analyses in function of IC BP-NGD PS physical parameters will be performed.

A. PGD AND NGD CHARACTERISATION

The synthesized CLC (which represents the PGD circuit) or and NGD circuits are characterized from the phase, $GD_{CLC,NGD}$, $S_{11CLC,NGD}$ and $S_{21CLC,NGD}$ analyses. As depicted by Figs. 15 and Figs. 16, the calculated and simulated results are in excellent correlation. Fig. 15(a) shows the comparison between:

- The calculated ("Calc.$_{CLC}$" plotted in black solid line) and ADS® simulated ("ADS$_{CLC}$" plotted in dotted blue-sky line) of the CLC-circuit alone. The phase presents a clear negative slope with phase shift $\varphi_{CLC}(f_0) \approx -90°$.
- The calculated ("Calc.$_{CLC}$" plotted in dashed red line) and ADS® simulated ("ADS$_{CLC}$" plotted in dotted navy-blue line) of the CLC-circuit alone. The phase presents a clear negative slope with phase shift $\varphi_{NGD}(f_0) \approx 0°$.

The corresponding GDs are displayed by Fig. 15(b) which shows NGD from $f_1 = 1.456$ GHz to $f_2 = 2.48$ GHz with $GD_{NGD}(f_0) \approx -61$ ps. The NGD effect compensates the PGD which presents $GD_{CLC}(f_0) \approx 165$ ps. Fig. 16(a) confirms that the CLC and NGD circuits are matched to $S_{11CLC,NGD}(f_0) \approx -13$ dB around the expected working frequency. Both circuits present transmission coefficients better than $S_{21CLC,NGD}(f_0) > -2$ dB as illustrated by Fig. 16(b) confirms that the CLC and NGD circuits. The results of the combined CLC and NGD circuits designed in 130-nm BiCMOS IC technology with parameters indicated by Table 2 and Table 3 are examined in the next subsection.

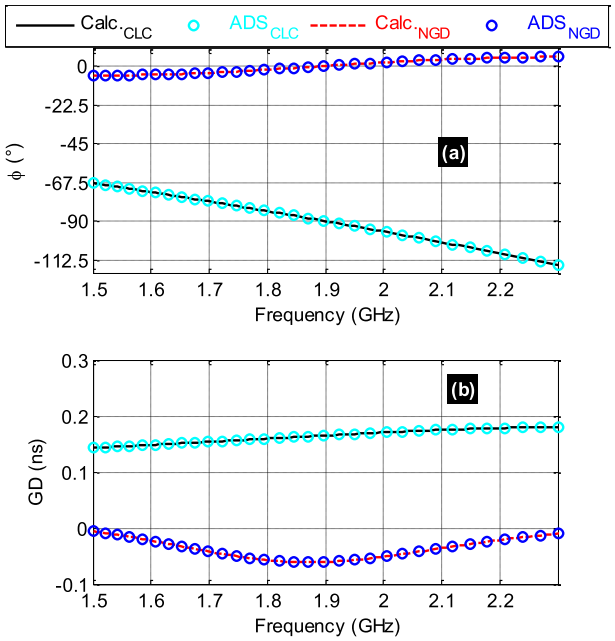

FIGURE 15. Comparison of calculated and simulated (a) phases and (b) GDs of the PGD and NGD circuits.

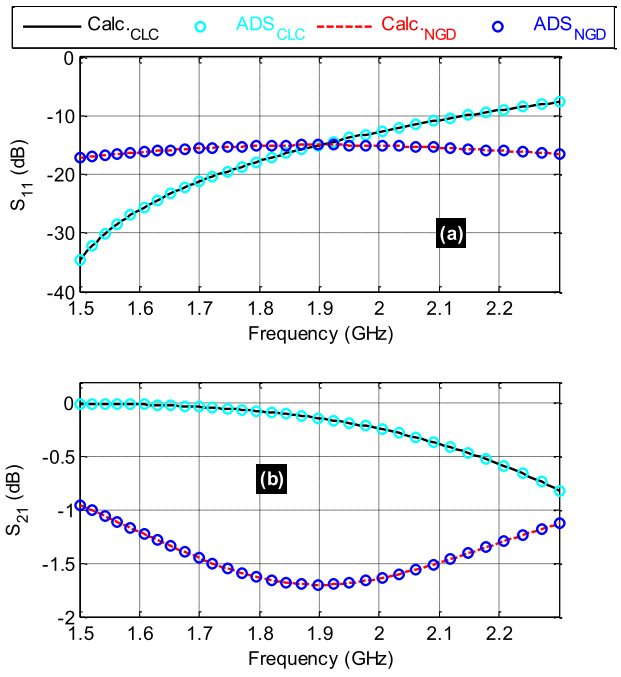

FIGURE 16. Comparison of calculated and simulated (a) S_{11} and (b) S_{21} of the PGD and NGD circuits.

B. BiCMOS IC DESIGNED BP-NGD CONSTANT PS VERICATION RESULT

The verification of the IC design feasibility was performed based on comparisons between:

- Calculated ("Model" plotted in black solid line) results from ideal model,
- ADS® simulated ("ADS" dotted in blue-sky dotted line) results from ideal schematic.
- CADENCE VIRTUOSO® simulated ("Cadence" dotted in blue-sky dotted line) results from BiCMOS IC layout.

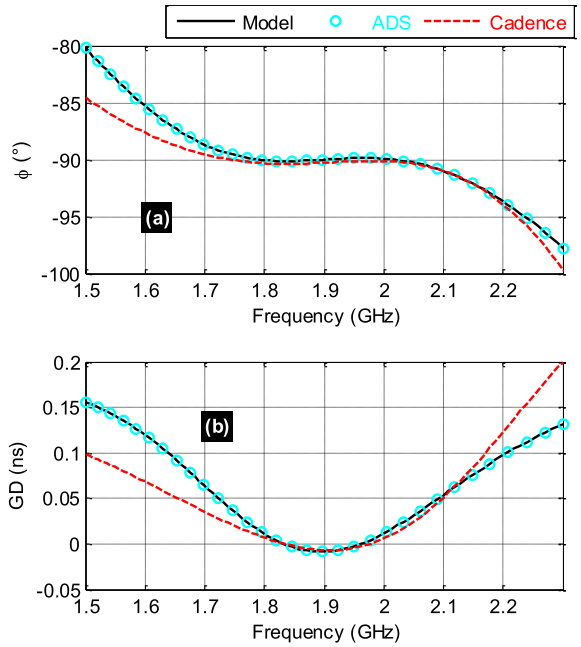

FIGURE 17. Comparison of calculated and simulated (a) phases and (b) GDs of the BP-NGD PS POC.

Fig. 17(a) displays the BP-NGD PS phase and the associated GDs are plotted in Fig. 17(b). A good agreement between the 130-nm BiCMOS designed BP-NGD PS POC and ideal ones (MATLAB® calculation and ADS® simulation) PSs and GDs are obtained.

As expected, they confirm undeniably the constant PS behavior with GD less than 10 ps around the working frequency. A good correlation of the behavior of the independent frequency phase shift around the working frequency $f_0 = 1.9$ GHz is shown in Fig. 17(a). Table 4 summarizes the BP-NGD PS specifications from the POCs of ideal and BiCMOS IC BP-NGD PS circuits shown in Figs. 12 and 14.

As results, we have the remarkable phase variations:

- $\Delta\varphi(f_0+/-\Delta f/2)=-90°\pm1°$ in the bandwidth delimited by $f_{low-PS} = 1.75$ GHz and $f_{high-PS} = 2.1$ GHz from ideal circuit,
- against $\Delta\varphi(f_0+/-\Delta f/2)= -90° \pm 0.4°$ in the bandwidth delimited by $f_{low-PS} = 1.7$ GHz and $f_{high-PS} = 2.05$ GHz from the BiCMOS POC.

In addition, the associated reflection and transmission coefficients of the BP-NGD PS are plotted in Figs. 18. They show a good access matching better than $S_{11}(f_0) < -15$ dB in the considered frequency band PS BW. Moreover, the PS flatness transmission coefficient is less than 1 dB. The main differences between S_{11} and S_{21} observed in Figs. 17 are due to the CMOS distributed component designed.

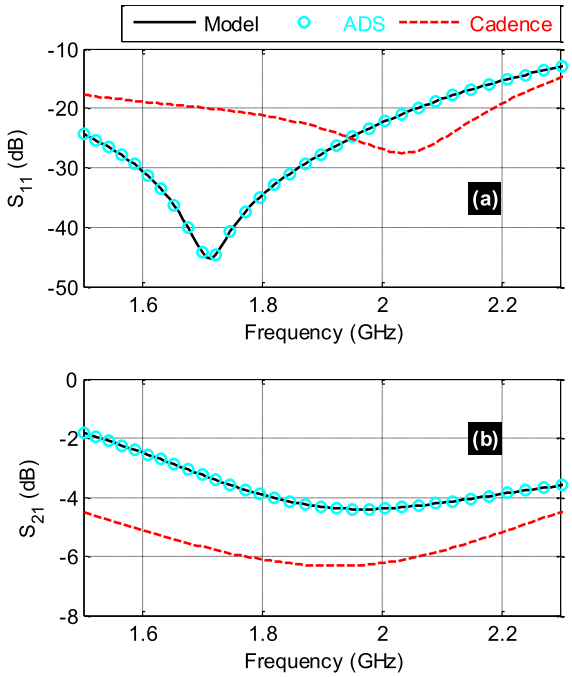

FIGURE 18. Comparison of calculated and simulated (a) S_{11} and (b) S_{21} of the BP-NGD PS POC.

To highlight the proposed design robustness of the 130-nm BiCMOS PS, MC UAs were run and the results are discussed in the following subsection.

C. MC UAS OF THE BiCMOS IC BP-NGD PS

The carried-out UAs were performed by considering the geometrical parameters of the implemented resistor and inductor by means of the PLS of BiCMOS IC PS. Based on statistical approach, all parameters are simultaneously changed under $+/-5\%$ variations. The references values of the resistor and inductor parameters are indicated by Table 2 and Table 3, respectively.

The following paragraphs are discussing the obtained CADENCE VIRTUOSO® based simulation results following the MC UAs with $n = 1000$-trials via Gaussian distribution statistical probability (DSP).

1) MC UA OF IC BP-NGD PS PHASE SHIFT AVERAGE IN THE CONSIDERED BW

In this first case of study, the UAs were based on the CADENCE-VIRTUOSO® simulations by considering $+/-5\%$ variations of the BP-NGD PS POCs initial parameters (through standard deviations). The obtained average phase shift denoted φ_{ave} from $f_{low-PS} = 1.7$ GHz and $f_{high-PS} = 2.05$ GHz was considered for the statistical analyses of the samples in the intervals delimited by the one, two and three times multiple of standard deviation. The statistical analyses from the computed results lead to the flat typical Gaussian variations with assessed values. Fig. 19 presents the histogram and DSP of φ_{ave} from BP-NGD PS chip POC. Significant probability of phase variation is observed from $-91.5°$ to $-89.5°$.

TABLE 5. Specifications of the considered ideal circuit and bicmos layout BP-NGD PS.

Parameters	Calculated	ADS®	Cadence®
f_{low-PS}	1.75 GHz	1.75 GHz	1.7 GHz
$f_{high-PS}$	2.1 GHz	2.1 GHz	2.05 GHz
$(f_{high-PS} - f_{low-PS})/f_0$	18.4%	18.4%	18.4%
$\varphi(f_0)$	-90°	-90°	-90.3°
$\Delta\varphi$ (°)	-90+/-1°	-90+/-1°	-90+/-0.4°
$\Delta S_{21}(f_0)$	-2.8+/-0.5 dB	-2.8+/-0.5 dB	-5.3+/-0.7 dB

2) PS GD AVERAGE

Like the previous case, the statistical analyses of GD were performed from the CADENCE® simulated results. All the physical parameters of the BiCMOS IC BP-NGD GD were varied in the same frequency band. The average value of the GD results from $f_{low-PS} = 1.7$ GHz and $f_{high-PS} = 2.05$ GHz enables to establish the accentuated Gaussian variations with assessed values. Fig. 20 presents the histogram of average value GD_{ave}. The GD mean value is of about 7 ps with high DSP over standard deviation 6.3 ps.

3) PS S_{21} AVERAGE

By means of the same MC UAs, the transmitted coefficient of the BP-NGD IC POS was analyzed. We assess then the average value if the transmission coefficient in the same previous bandwidth from f_{low-PS} and $f_{high-PS}$. Fig. 21 displays the histogram and DSP of S_{21ave}. The mean statistical value is of about -6.11 dB over standard deviation of about 0.6 dB.

4) PS S_{11} MAXIMUM

The last case MC UA of BP-NGD PS POC UA is focused on the reflection coefficient. The analysis is based on the assessment of maximum $S_{11\max} = \max[S_{11}(f)]$. Fig. 22 depicts the histogram and DSP of S_{11ave}. We can emphasize that mean value is of about -9.1 dB over the standard deviation of about 1.1 dB. This result enables to state that our BiCMOS PS presents a risk of unmatching if the physical parameters varied over $+/-5\%$ relative variation.

5) SUMMARY OF MEAN AND STANDART DEVIATION

Based on the previous results, Table 5 addresses the summary of the MC UAs. We recall that the statistical run was repeated with 1000 trials.

The last explored table indicates the mean values and standard deviations of the four previously discussed specific characteristics analyzed. Less relative variation of physical parameters should be expected to ensure BP-NGD phase shift respecting the criteria of microwave circuits in $f_{low-PS} = 1.7$ GHz and $f_{high-PS} = 2.05$ GHz.

D. PERFORMANCE COMPARISON OF BP-NGD BASED PS

Similar to the investigation on unfamiliar BP-NGD circuit design, the relevance of the proposed BiCMOS BP-NGD PS can be understood with bibliographic study. Table 6 addresses a comparison of performances of unfamiliar BP-NGD circuit-based frequency independent PSs available in the literature

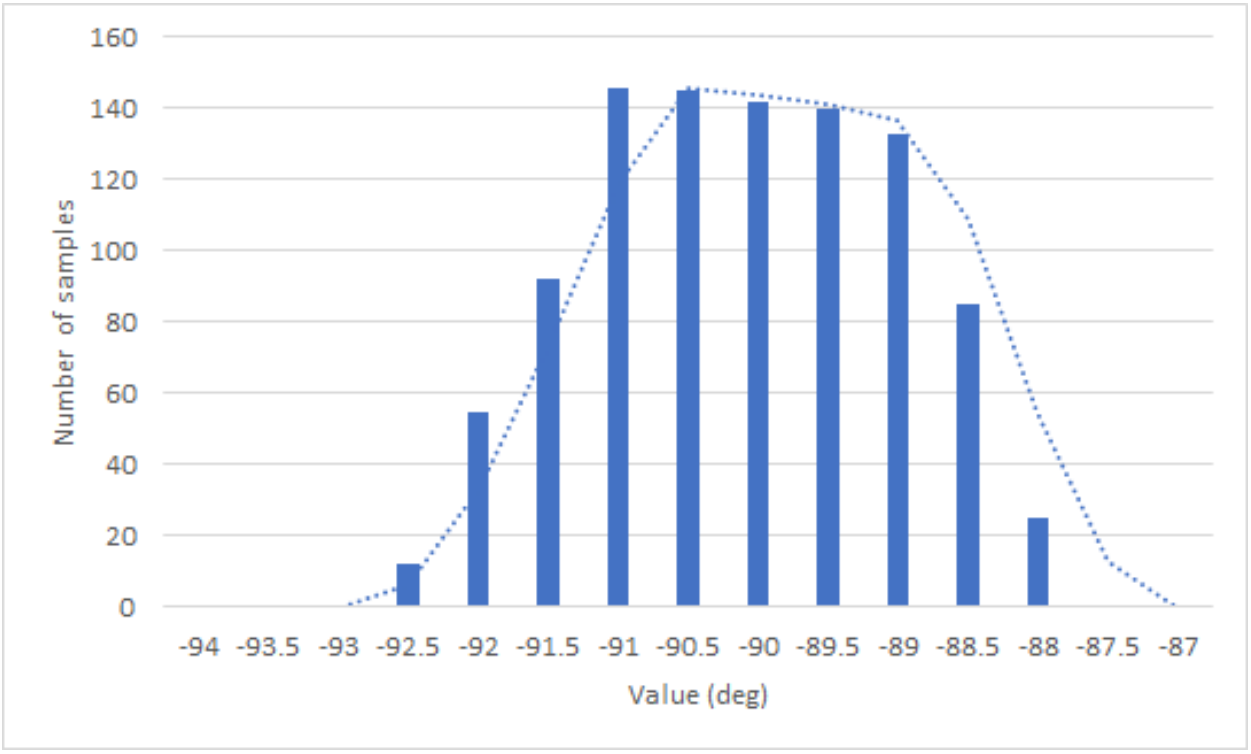

FIGURE 19. Histogram of $\varphi_{ave}(f)$ average from the BP-NGD PS MC UA.

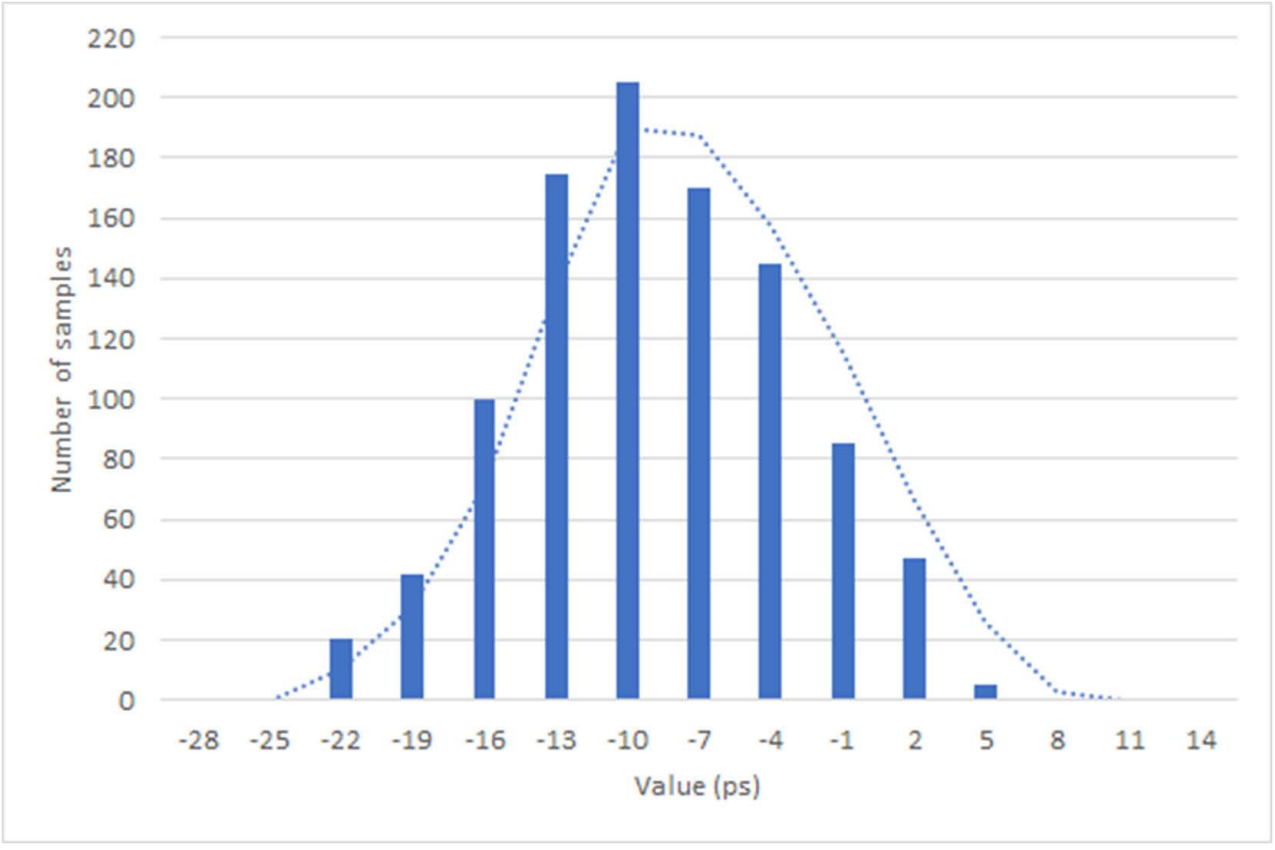

FIGURE 20. Histogram of GD_{PS} average from the BP-NGD PS MC UA.

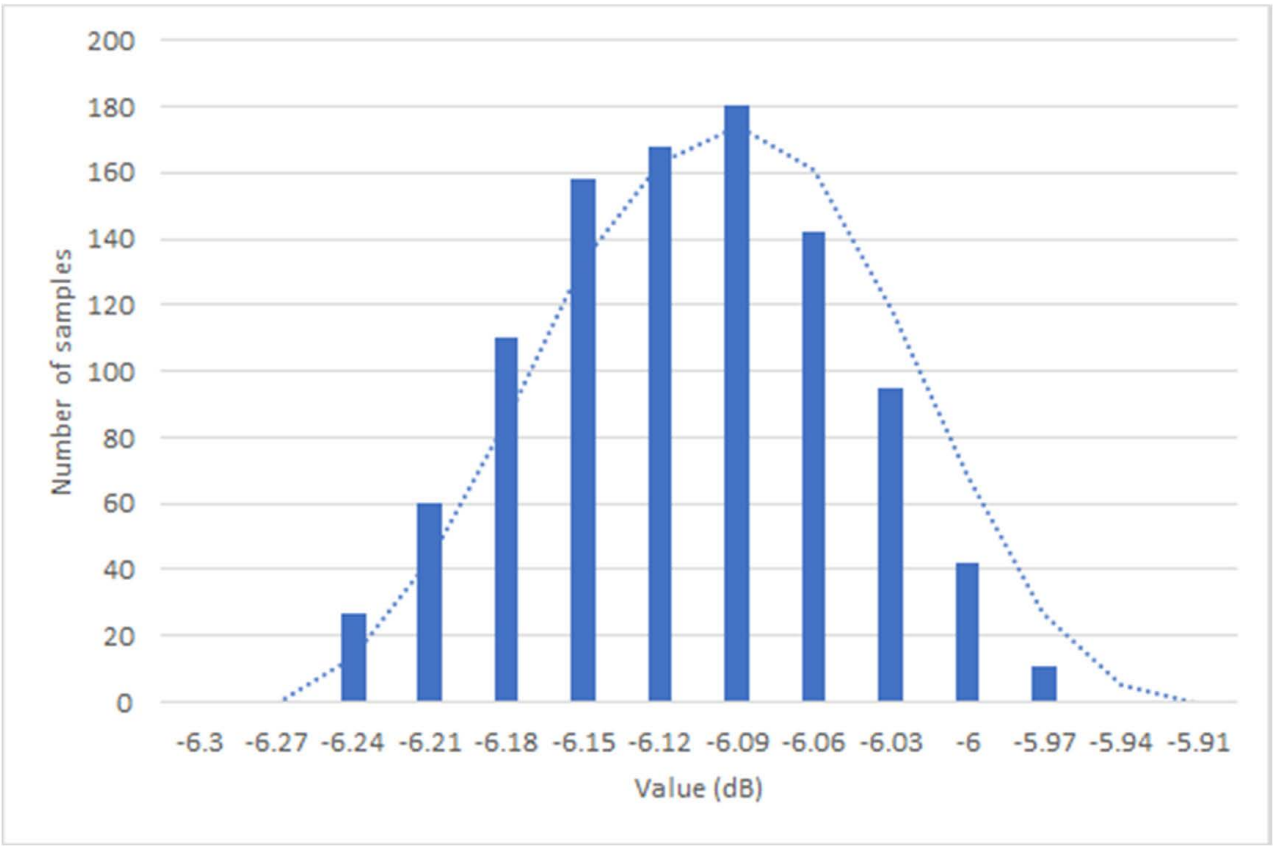

FIGURE 21. Histogram of $S_{21ave}(f)$ average from the BP-NGD PS MC UA.

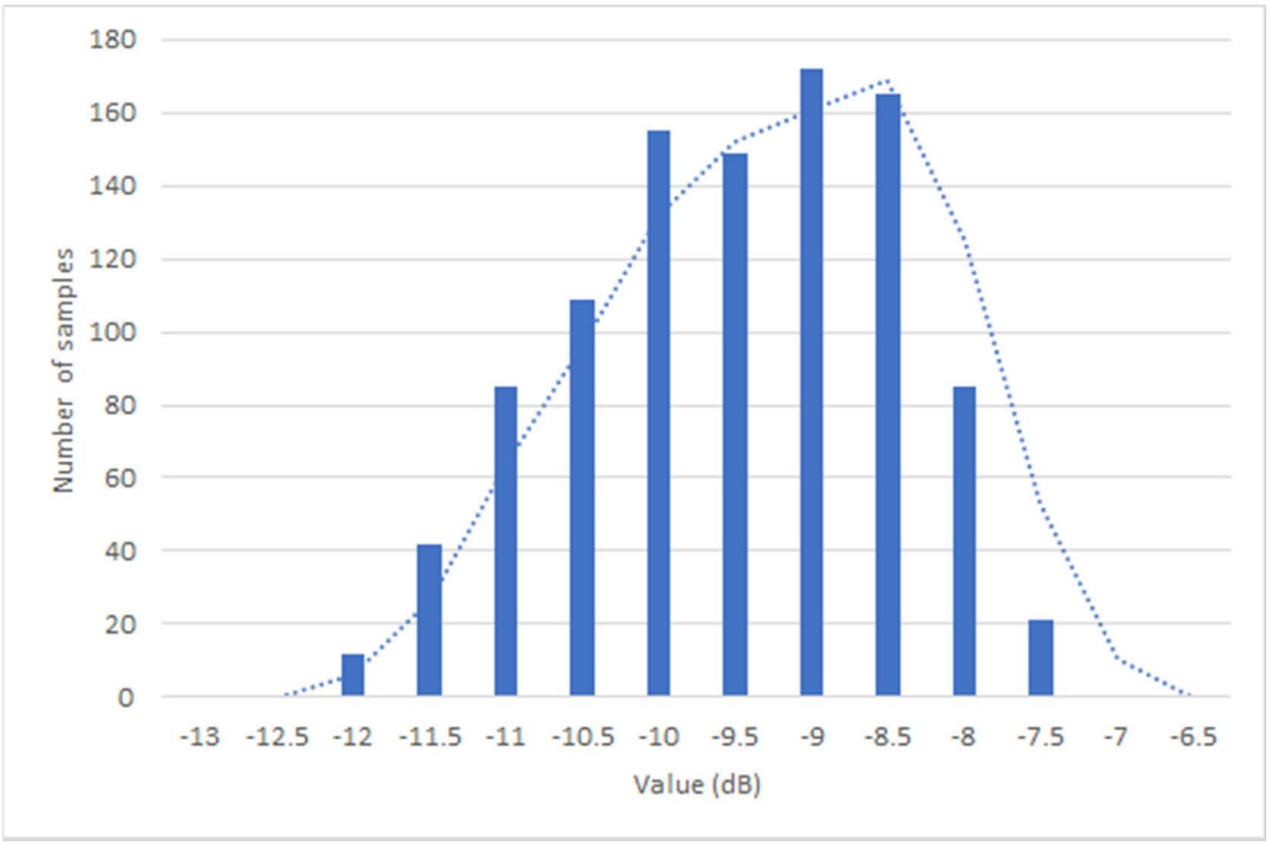

FIGURE 22. $S_{11max}(f_0)$ histogram from the BP-NGD PS MC UA.

TABLE 6. IC BP-NGD PS mean and standard deviations from n=1000 trial UAs.

PS characteristics	Statistical parameter	Value
φ_{ave}	Mean	-90.48°
	Standard deviation	0.98°
GD_{ave}	Mean	7 ps
	Standard deviation	6.3 ps
S_{21ave}	Mean	-6.11 dB
	Standard deviation	0.63 dB
S_{11max}	Mean	-9.1 dB
	Standard deviation	1.1 dB

TABLE 7. Comparison of performances of BP-NGD based RF and microwave PS.

Ref.	Design technology	f_{min} (GHz)	f_{max} (GHz)	Φ_{mean} (°)	$\Delta\Phi$ (°)	$\Delta S_{21}(f_o)$ (dB)
[29]	Hybrid microstrip	1.08	2.42	90	+/-5	0+/-2
[30]		0.102	0.935	145	+/-10	2+/-2
[32]		4.1	6.8	90	+/-10	2.5+/-2.5
[33]		0.675	1..375	-180	+/-5	-18.4 to -15.4
		0.572	1.432	-90	+/-3	-12.8 to -9.8
		0.742	1.3	90	+/-4	-19.7 to -16.7
[34]	Lumped	1.114	1.333	-120	+/-5	-3.72+/-1.42
[35]	Hybrid microstrip	2	2.3	-70	+/-4	0.88
		2.6	2.9	-104	+/-2	0.94
The presented BP-NGD PS	130-nm BiCMOS	1.7	2.05	-90.3	+/-0.4	0.7

[29], [30], [32], [33], [34], [35]. They are dedicated to operate in RF and microwave frequencies and implemented with lumped (using R, L, C and transistor components), microstrip and hybrid technologies. It is worth to note that according to the state-of-the-art, there are different topologies BP-NGD circuit-based PS which are implemented either with passive or active circuits. Most of existing PSs were designed to operate in single-band [29], [30], [32], [33], [34] and one of them operates in dual-band [35].

The proposed BiCMOS BP-NGD PS presents a remarkable advantage in terms of phase shift and transmission coefficient flatness's. Furthermore, it is the first time that this particular microwave PS was designed in miniature technology based on 130-nm BiCMOS which allows to reach physical size lower than 1 mm^2.

VIII. CONCLUSION

An original research work on BP-NGD microwave engineering application for designing miniature quadrature passive PS operating independently to the frequency is developed. The investigated PS IC using unfamiliar BP-NGD function is innovatively designed in 130-nm BiCMOS technology.

The theoretical approach based on the S-matrix modelling is elaborated. The main principle of the BP-NGD PS topology is implemented from the cascade of PGD and NGD circuits. The PGD circuit is constituted by inductor and capacitor which named CLC reactive network. The NGD one is composed of RLC-resonant network. The modelling, analysis and synthesis of BP-NGD and CLC PGD are introduced. The synthesis equations enabling to determine the lumped circuit parameters in function of the targeted working frequency, phase shift, GD and reflection coefficient are established.

To generalize the BP-NGD PS concept in BiCMOS technology, the design methodology of IC including the DRC, LVS and PLS is described. The design feasibility of the miniaturized BP-NGD PS is verified in 130-nm BiCMOS technology by using a standard commercial tool. The obtained results confirm the IC designability of the BP-NGD PS. As expected, the constant phase shift of about $-90+/-1°$ with outstanding challenging flatness is obtained. Moreover, the PS flatness is verified over 18.4% relative bandwidth. Furthermore, interesting flatness's of transmission coefficient phase and magnitude is verified. The robustness of the PS expected during the fabrication process is expected with 1000-trial MC UAs. The sensitivities of the constant PS characteristics are pointed out in function of the relative variations of layout IC physical parameters.

As ongoing research in continuation of the present study, we are currently working on:

- The fabrication and test of BiCMOS BP-NGD PS prototypes,
- The feasibility of BP-NGD PS at higher frequencies as W-band,
- The integration and test of multi-band BP-NGD PS in for phased array antenna design [40], [41], [42], [43],
- And the real environment characterization test of miniaturized CMOS and MMIC PS for the future 5G and 6G TxRx microwave system.

REFERENCES

[1] B. Ségard and B. Macke, "Observation of negative velocity pulse propagation," *Phys. Lett. A*, vol. 109, pp. 213–216, May 1985.
[2] J. N. Munday and W. M. Robertson, "Observation of negative group delays within a coaxial photonic crystal using an impulse response method," *Opt. Commun.*, vol. 273, no. 1, pp. 32–36, 2007.
[3] B. Macke and B. Ségard, "Two-pulse interference and superluminality," *Opt. Commun.*, vol. 281, no. 1, pp. 12–17, Jan. 2008.
[4] G. V. Eleftheriades, O. Siddiqui, and A. K. Iyer, "Transmission line for negative refractive index media and associated implementations without excess resonators," *IEEE Microw. Wireless Compon. Lett.*, vol. 13, no. 2, pp. 51–53, Feb. 2003.
[5] O. F. Siddiqui, M. Mojahedi, and G. V. Eleftheriades, "Periodically loaded transmission line with effective negative refractive index and negative group velocity," *IEEE Trans. Antennas Propag.*, vol. 51, no. 10, pp. 2619–2625, Oct. 2003.
[6] Z. Wang, Y. Cao, T. Shao, S. Fang, and Y. Liu, "A negative group delay microwave circuit based on signal interference techniques," *IEEE Microw. Wireless Compon. Lett.*, vol. 28, no. 4, pp. 290–292, Apr. 2018.
[7] B. Ravelo and S. De Blasi, "An FET-based microwave active circuit with dual-band negative group delay," *J. Microw., Optoelectron. Electromagn. Appl.*, vol. 10, no. 2, pp. 355–366, Dec. 2011.
[8] B. Ravelo, "Innovative theory on multiband NGD topology based on feedback-loop power combiner," *IEEE Trans. Circuits Syst. II, Exp. Briefs*, vol. 63, no. 8, pp. 738–742, Aug. 2016.
[9] X. Zhou, B. Li, N. Li, B. Ravelo, X. Hu, Q. Ji, F. Wan, and G. Fontgalland, "Analytical design of dual-band negative group delay circuit with multi-coupled lines," *IEEE Access*, vol. 8, pp. 72749–72756, 2020.

[10] G. Liu and J. Xu, "Compact transmission-type negative group delay circuit with low attenuation," *Electron. Lett.*, vol. 53, no. 7, pp. 476–478, Mar. 2017.
[11] T. Shao, Z. Wang, S. Fang, H. Liu, and S. Fu, "A compact transmission line self-matched negative group delay microwave circuit," *IEEE Access*, vol. 5, pp. 22836–22843, 2017.
[12] T. Shao, S. Fang, Z. Wang, and H. Liu, "A compact dual-band negative group delay microwave circuit," *Radioengineering*, vol. 27, no. 4, pp. 1070–1076, Dec. 2018.
[13] B. Ravelo, "Similitude between the NGD function and filter gain behaviours," *Int. J. Circuit Theory Appl.*, vol. 42, no. 10, pp. 1016–1032, Oct. 2014.
[14] B. Ravelo, "On the low-pass, high-pass, bandpass and stop-band NGD RF passive circuits," *URSI Radio Sci. Bull.*, vol. 2017, no. 363, pp. 10–27, Dec. 2017.
[15] B. Ravelo, "First-order low-pass negative group delay passive topology," *Electron. Lett.*, vol. 52, no. 2, pp. 124–126, Jan. 2016.
[16] R. Randriatsiferana, Y. Gan, F. Wan, W. Rahajandraibe, R. Vauché, N. M. Murad, and B. Ravelo, "Study and experimentation of a 6-dB attenuation low-pass NGD circuit," *Anal. Integr. Circuits Signal Process.*, vol. 110, no. 1, pp. 105–114, Jan. 2022.
[17] E. J. R. Sambatra, A. Jaomiary, S. Ngoho, S. S. Yazdani, N. M. Murad, G. Chan, and B. Ravelo, "Low-pass negative group delay modelling and experimentation with tri-port resistorless passive cross-circuit," *Prog. Electromagn. Res. M*, vol. 108, pp. 39–51, 2022.
[18] M. Guerin, F. Wan, K. Gorshkov, X. Huang, B. Tishchuk, F. E. Sahoa, G. Chan, S. Baccar, W. Rahajandraibe, and B. Ravelo, "High-pass NGD characterization of resistive-inductive network based low-frequency circuit," *COMPEL-Int. J. Comput. Math. Electr. Electron. Eng.*, vol. 40, no. 5, pp. 1032–1049, Oct. 2021.
[19] R. Yang, X. Zhou, S. S. Yazdani, E. Sambatra, F. Wan, S. Lallechere, and B. Ravelo, "Analysis, design and experimentation of high-pass negative group delay lumped circuit," *Circuit World*, to be published, doi: 10.1108/CW-07-2020-0131.
[20] S. Fenni, F. Haddad, A. Jaomiary, S. S. Yazdani, F. E. Sahoa, L. Ramifidisoa, M. Guerin, W. Rahajandraibe, and B. Ravelo, "Investigation on four-port mono-capacitor circuit with high-pass negative group delay behavior," *Int. J. Circuit Theory Appl.*, vol. 50, no. 2, pp. 478–495, Feb. 2022.
[21] H. Jia, F. Wan, J. Frnda, M. Guerin, W. Rahajandraibe, P. Thakur, A. Thakur, B. Agnus, and B. Ravelo, "Novel tee-shaped topology theory of low- and high-pass NGD double-type function," *IEEE Access*, vol. 10, pp. 28445–28460, 2022.
[22] M. Guerin, Y. Liu, A. Douyere, G. Chan, F. Wan, S. Lallechere, W. Rahajandraibe, and B. Ravelo, "Design and synthesis of inductorless passive cell operating as stop-band negative group delay function," *IEEE Access*, vol. 9, pp. 100141–100153, 2021.
[23] S. Fenni, F. Haddad, K. Gorshkov, B. Tishchuk, A. Jaomiary, F. Marty, G. Chan, M. Guerin, W. Rahajandraibe, and B. Ravelo, "AC low-frequency characterization of stopband negative group delay circuit," *Prog. Electromagn. Res. C*, vol. 115, pp. 261–276, 2021.
[24] J.-K. Xiao, Q.-F. Wang, and J.-G. Ma, "Negative group delay circuits and applications: Feedforward amplifiers, phased-array antennas, constant phase shifters, non-foster elements, interconnection equalization, and power dividers," *IEEE Microw. Mag.*, vol. 22, no. 2, pp. 16–32, Feb. 2021.
[25] C. D. Broomfield and J. K. A. Everard, "Broadband negative group delay networks for compensation of oscillators, filters and communication systems," *Electron. Lett.*, vol. 36, no. 23, pp. 1931–1933, Nov. 2000.
[26] K.-P. Ahn, R. Ishikawa, and K. Honjo, "Group delay equalized UWB InGaP/GaAs HBT MMIC amplifier using negative group delay circuits," *IEEE Trans. Microw. Theory Techn.*, vol. 57, no. 9, pp. 2139–2147, Sep. 2009.
[27] B. Ravelo, S. Lalléchère, A. Thakur, A. Saini, and P. Thakur, "Theory and circuit modeling of baseband and modulated signal delay compensations with low-and band-pass NGD effects," *AEU-Int. J. Electron. Commun.*, vol. 70, no. 9, pp. 1122–1127, Sep. 2016.
[28] T. Shao, Z. Wang, S. Fang, H. Liu, and Z. N. Chen, "A full-passband linear-phase band-pass filter equalized with negative group delay circuits," *IEEE Access*, vol. 8, pp. 43336–43343, 2020.
[29] B. Ravelo, M. Le Roy, and A. Perennec, "Application of negative group delay active circuits to the design of broadband and constant phase shifters," *Microw. Opt. Technol. Lett.*, vol. 50, no. 12, pp. 3077–3080, Dec. 2008.
[30] B. Ravelo, A. Pérennec, and M. Le Roy, "Synthesis of frequency-independent phase shifters using negative group delay active circuit," *Int. J. RF Microw. Comput.-Aided Eng.*, vol. 21, no. 1, pp. 17–24, Jan. 2011.
[31] B. Ravelo, M. Le Roy, and A. Pérennec, "Frequency-independent active phase shifters for UWB applications," in *Proc. 40th Eur. Microw. Conf.*, Paris, France, Sep. 2010, pp. 1774–1777.
[32] B. Ravelo, "Distributed NGD active circuit for RF-microwave communication," *AEU-Int. J. Electron. Commun.*, vol. 68, no. 4, pp. 282–290, Apr. 2014.
[33] Y. Meng, Z. Wang, S.-J. Fang, and H. Liu, "Broadband phase shifter with constant phase based on negative group delay circuit," *Prog. Electromagn. Res. Lett.*, vol. 103, pp. 161–169, 2022.
[34] J. Nebhen and B. Ravelo, "Innovative microwave design of frequency-independent passive phase shifter with LCL-network and bandpass NGD circuit," *Prog. Electromagn. Res. C*, vol. 109, pp. 187–203, 2021.
[35] B. Ravelo, G. Fontgalland, H. S. Silva, J. Nebhen, W. Rahajandraibe, M. Guerin, G. Chan, and F. Wan, "Original application of stop-band negative group delay microwave passive circuit for two-step stair phase shifter designing," *IEEE Access*, vol. 10, pp. 1493–1508, 2022.
[36] B. Ravelo, "Negative group delay based Hilbert filter," in *Negative Group Delay Devices: From Concept to Applications*, Hertfordshire, U.K.: Michael Faraday House, 2018, ch. 7, pp. 173–198.
[37] M. A. Antoniades and G. V. Eleftheriades, "Compact linear lead/lag metamaterial phase shifters for broadband applications," *IEEE Antennas Wireless Propag. Lett.*, vol. 2, pp. 103–106, 2003.
[38] Y. Li, M. F. Iskander, Z. Zhang, and Z. Feng, "A new low cost leaky wave coplanar waveguide continuous transverse stub antenna array using metamaterial-based phase shifters for beam steering," *IEEE Trans. Antennas Propag.*, vol. 61, no. 7, pp. 3511–3518, Jul. 2013.
[39] S. S. Oh and L. Shafai, "Compensated circuit with characteristics of lossless double negative materials and its application to array antennas," *IET Microw., Antennas Propag.*, vol. 1, no. 1, pp. 29–38, Feb. 2007.
[40] H. Liu, S. Gao, and T. H. Loh, "Compact dual-band antenna with electronic beam-steering and beamforming capability," *IEEE Antennas Wireless Propag. Lett.*, vol. 10, pp. 1349–1352, 2011.
[41] B. Ravelo, W. Rahajandraibe, M. Guerin, B. Agnus, P. Thakur, and A. Thakur, "130-nm BiCMOS design of low-pass negative group delay integrated RL-circuit," *Int. J. Circuit Theory Appl.*, vol. 50, no. 6, pp. 1876–1889, Jun. 2022.
[42] F. Wan, T. Gu, B. Li, B. Li, W. Rahajandraibe, M. Guerin, S. Lallechere, and B. Ravelo, "Design and experimentation of inductorless low-pass NGD integrated circuit in 180-nm CMOS technology," *IEEE Trans. Comput.-Aided Design Integr. Circuits Syst.*, early access, Dec. 23, 2021, doi: 10.1109/TCAD.2021.3136982.
[43] M. Guerin, W. Rahajandraibe, G. Fontgalland, H. S. Silva, G. Chan, F. Wan, P. Thakur, A. Thakur, J. Frnda, and B. Ravelo, "Theory and original design of resistive-inductive network high-pass negative group delay integrated circuit in 130-nm CMOS technology," *IEEE Access*, vol. 10, pp. 27147–27161, 2022.

BLAISE RAVELO (Member, IEEE) is currently an University Full Professor at NUIST, Nanjing, China. He is also a Lecturer in circuit & system theory, science, technology, engineering and mathematics (STEM), and applied physics. He is also a Pioneer of the Negative Group Delay (NGD) concept about t<0 signal traveling physical space. This extraordinary concept is potentially useful for anticipating and prediction all kind of information. He was the research director of 11 Ph.D. students (ten defended), a postdoctoral researcher, a research engineer, and master's internships. With U.S., Chinese, Indian, European, and African partners, he is actively involved and contributes on several international research projects (ANR, FUI, FP7, INTERREG, H2020, and Euripides^2, Eurostars). He is the coauthor of more than 370 scientific research papers in new technologies published in international conferences and journals. His research interests include multiphysics and electronics engineering. He is a member of *IET Electronics Letters* Editorial Board as a Circuit & System Subject Editor.

He has been a member of Scientific Technical Committee of Advanced Electromagnetic Symposium (AES), since 2013. He is ranked in Top 2% world's scientists based on years (2020–2021) by Stanford University, USA (https://elsevier.digitalcommonsdata.com/datasets/btchxktzyw/3). He has Google Scholar H-index (2022)=26 and i10-index (2022)=83. He is also a member of research groups, such as URSI, GDR Ondes, and Radio Society. He regularly invited to review papers submitted for publication to international journals, such as IEEE TRANSACTIONS ON MICROWAVE THEORY AND TECHNIQUES, IEEE TRANSACTIONS ON CIRCUITS AND SYSTEMS, IEEE TRANSACTIONS ON ELECTROMAGNETIC COMPATIBILITY, IEEE TRANSACTIONS ON INDUSTRIAL ELECTRONICS, IEEE ACCESS, *IET CDS*, and *IET MAP*, and books (Wiley, Intech Science).

MATHIEU GUERIN (Member, IEEE) received the Doctorate (Engineering) degree in microelectronics and telecommunications from Polytech Marseille, in 2010. He was a Research Master in integrated circuits design with the University of Aix-Marseille, in 2010. He worked as the Technical Leader of the Analog and Radio-Frequency Design Team, IDEMIA-StarChip, for five years and designed chips embedded in SIM cards and contactless bank cards with biometric recognition. He joined Aix-Marseille University as an Assistant Professor, in 2020, and he joined the IM2NP Laboratory, CCSI Team. He is also working on methods of modeling and characterizing circuits in analog electronics. His research interests include the design and synthesis of circuits in digital electronics.

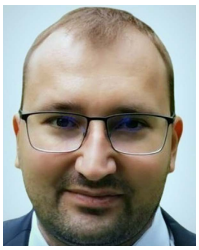

JAROSLAV FRNDA (Senior Member, IEEE) was born in Slovakia, in 1989. He received the M.Sc. and Ph.D. degrees from the Department of Telecommunications, VSB—Technical University of Ostrava, Czechia, in 2013 and 2018, respectively. He is currently working as an Assistant Professor at the University of Zilina, Slovakia. He has authored or coauthored 32 SCI-E and nine ESCI papers in WoS. His research interests include quality of multimedia services in IP networks, data analysis, and machine learning algorithms.

FRANK ELLIOT SAHOA received the master's degree in electrical engineering from the University of Antsiranana, Madagascar, in 2004, and the master's degree in nuclear physics, theoretical physics, and applied physics from the University of Antananarivo, in 2007. From 2008 to 2010, he was a DAAD Doctorate Fellow of the Institüt für Nukleare Entsorgung (I.N.E.), Karlsruhe Institute of Technology—Germany. He defended his Ph.D. thesis at the University of Antananarivo, in 2015, where he is currently an Assistant Professor at the Physics Department. His research interests include environmental radioactivity monitoring using nuclear techniques and negative group delay (NGD) circuits. He is regularly involved to participate in international technical cooperation projects supported by IAEA, such as MAG/7/002, MAG/5/014, RAF/5/063, and MAG/5/019.

GLAUCO FONTGALLAND (Senior Member, IEEE) was born in Fortaleza, Ceará, Brazil, in March 1966. He received the Graduate and M.S. degrees in electrical engineering from the Universidade Federal de Campina Grande (UFCG), Campina Grande—Paraíba, Brazil, in 1990 and 1993, respectively, and the Ph.D. degree in electronics from the Toulouse Institut National Polytechnique—ENSEEIHT, Toulouse, France, in 1999.

His Ph.D. thesis work was nominated at the Toulouse Institut National Polytechnique—ENSEEIHT for the Leopold Escande Award, in 1999. From 2010 to 2012, he was a Visiting Scholar at the ElectroScience Laboratory, The Ohio State University (OSU), USA. Currently, he is a Full Professor at UFCG, where he develops research on: electromagnetic modeling, EMC, EMI, ESD, RFID, UWB, propagation, and antennas for various applications. He has published more than 200 papers in journals and conferences.

Dr. Fontgalland is a member of the Sociedade Brasileira de Micro-ondas e Optoeletrônica (SBMO), Sociedade Brasileira de Eletromagnetismo (SBMag), Sociedade Brasileira de Microeletrôncia (SBMicro), and The applied Computacional Eletromagnetics Society (ACES). He is the Past IEEE AP-S Chapter Chair and a member of the 2020 IEEE AP-S Student Design Contest and 2020 IEEE AP-S Field Awards Evaluation. Since 2019, he has been an Associate Editor of IEEE LATIN AMERICA TRANSACTIONS.

HUGERLES S. SILVA (Member, IEEE) received the B.Sc., M.Sc., and Ph.D. degrees in electrical engineering from UFCG, Brazil, in 2014, 2016, and 2019, respectively. He is currently pursuing the Ph.D. degree with the Telecommunications Institute, University of Aveiro, Portugal. His research interests include wireless communications, digital signal processing, and wireless channel modeling.

SAMUEL NGOHO received the Graduate degree from ESIGELEC, Rouen, France, in 2012, and the Ph.D. degree in thematic of high frequency electronics, photonics and systems from the XLIM Laboratory, University of Limoges, Limoges, France. His Ph.D. subject concerned was based on the design and production of integrated optoelectronic components for high speed telecommunications systems. He worked as an Integration, Verification, Validation, and Qualification Engineer of RF/HF products and systems for civil and military applications. He is currently working as a System Engineer at THALES SIX, Gennevilliers, France. His research interests include the progress of microelectronics, in particular in the development of innovative functions integrated in microwave devices to meet the need for densification and evolution of spectra for future communications systems. He also takes part within research groups in the use of unfamiliar methods for resolving complex system as Kron's method.

FAYROUZ HADDAD (Member, IEEE) received the master's degree in electronic engineering from ENSEIRB, Bordeaux, France, in 2006, and the Ph.D. degree in microelectronics from Aix-Marseille University (AMU), France, in 2009.

Since 2010, she has been with the Integrated Circuits Design Team, Institute of Materials, Microelectronics and Nanosciences of Provence (IM2NP), Marseille, France. She is currently an Assistant Professor at AMU. She co-supervised eight master's and five Ph.D. students. She is the author or coauthor of more than 70 papers published in refereed journals and conferences. Her research interests include CMOS analog and RF integrated circuits design, ultra-low power (ULP), and multi-standards applications. She co-organized the International Conferences ICECS 2014 and NEWCAS 2021. She was a member of the technical program committee of several IEEE international conferences. She is a Reviewer of IEEE TRANSACTIONS ON CIRCUITS AND SYSTEMS (TCAS), *International Journal of Electronics and Communications* (AEUE), *Applied Sciences* journal, *IET Electronics Letters*, and for many IEEE conferences dedicated to integrated circuits (ISCAS, NEWCAS, ICECS, MWSCAS, ICMCS, and SBCCI).

WENCESLAS RAHAJANDRAIBE (Member, IEEE) received the B.Sc. degree in electrical engineering from Nice Sophia-Antipolis University, France, in 1996, the M.Sc. degree (Hons.) in electrical engineering from the Science Department, University of Montpellier, France, in 1998, and the Ph.D. degree in microelectronics from the University of Montpellier. He is currently a Full Professor at the University of Aix-Marseille. Since 1998, he has been with the Informatics, Robotics and Microelectronics Laboratory of Montpellier (LIRMM), Microelectronics Department. Since 2003, he has been with the Materials, Microelectronics and Nanoscience Laboratory of Provence (IM2NP), Microelectronic Department, Marseille, France, where he was an Associate Professor. Since 2014, he has been a Professor at Aix-Marseille University, where he heads the IM2NP Laboratory, Integrated Circuit Design Group. He is regularly involved to participate and to lead national and international research projects (ANR, H2020, and FP7 KIC-InnoEnergy). He directed and co-supervised 15 master's and 18 Ph.D. students. He is the author or coauthor of 11 patents and more than 150 papers published in refereed journals and conferences. He is an Expert of ANR and the French Agency for Research. His current research interests include AMS and RF circuit design from transistor to architectural level, ultralow power circuit design for smart sensor interface and embedded electronic in bioelectronic and e-health applications, wireless systems, design technique, and architecture for multi-standard transceiver. He has served on Program Committees for IEEE NEWCAS and ICECS. He has been and is a Reviewer of contributions submitted to several IEEE conferences and journals, such as ISCAS, NEWCAS, MWSCAS, ESSCIRC, ESSDERC, RFIC, IEEE TRANSACTIONS ON CIRCUITS AND SYSTEMS—I: REGULAR PAPERS, IEEE TRANSACTIONS ON CIRCUITS AND SYSTEMS—II: EXPRESS BRIEFS, and *IET Electronics Letters*.